**WSRC-TR-2003-00504, Rev. 0**
**Distribution Category: Unlimited**

**Keywords:** DWPF, refractory corrosion, metal corrosion, liquidus, crystallization, pouring

**Retention: Permanent**

# CHARACTERIZATION OF DEFENSE WASTE PROCESSING FACILITY (DWPF) GLASS AND DEPOSIT SAMPLES FROM MELTER #2 (U)

**C. M. Jantzen**
**A. D. Cozzi**
**N. E. Bibler**

**Publication Date: March 1, 2004**

**Approved by:**

**E.W. Holtzscheiter, Research Manager**
**Immobilization Technology Section**

**Westinghouse Savannah River Company**
**Savannah River Site**
**Aiken, SC 29808**


**PREPARED FOR THE U.S. DEPARTMENT OF ENERGY UNDER CONTRACT NO. DE-AC09-96SR18500**

**WSRC-TR-2003-00504, Rev. 0**
**Distribution Category: Unlimited**

**Keywords:** DWPF, refractory corrosion, metal corrosion, liquidus, crystallization, pouring

**Retention: Permanent**

# CHARACTERIZATION OF DEFENSE WASTE PROCESSING FACILITY (DWPF) GLASS AND DEPOSIT SAMPLES FROM MELTER #2 (U)

**C. M. Jantzen**
**A. D. Cozzi**
**N. E. Bibler**

**Publication Date: March 1, 2004**

**Approved by:**

**E.W. Holtzscheiter, Research Manager**
**Immobilization Technology Section**

**Westinghouse Savannah River Company**
**Savannah River Site**
**Aiken, SC 29808**

Savannah River Technology Center
SRTC
We Put Science to Work

**PREPARED FOR THE U.S. DEPARTMENT OF ENERGY UNDER CONTRACT NO. DE-AC09-96SR18500**

**This page was intentionally left blank**

## EXECUTIVE SUMMARY

The Defense Waste Processing Facility (DWPF) Engineering requested characterization of three glass samples that were taken from Melter #2 after the waste loading had been increased, e.g. after the new quasicrystalline liquidus model had been implemented and after DWPF switched from processing with Frit 200 to Frit 320. These samples were taken after DWPF observed very rapid buildup of deposits in the upper pour spout bore and on the pour spout insert while processing the high waste loading (~38 wt% feedstock). Rapid deposition in these locations had not occurred prior to this and, in turn, stopped after waste loading decreased. These samples were evaluated at SRTC using various analytical techniques for potential impacts on pouring problems recently experienced by the DWPF.

The pour stream sample was determined to be homogenous, amorphous, and representative of SME/MFT batch 245. The calculated viscosity from the pour stream analysis was within 2.5 poise of the MFT-245 Product Composition Control System (PCCS) prediction. The calculated liquidus from the pour stream analysis was within 10°C of the MFT-245 PCCS prediction. The glass REDOX was within 0.03 of the target and the waste loading (based on the reported $Li_2O$) was within 3.8 wt% of the MFT-245 target. This indicated that the viscosity, liquidus, and REDOX models are keeping DWPF processing in control. There was no crystallization observed in the pour stream sample.

The most likely mechanism by which the severe crystallization of the pour spout and insert occurred are the temperature and oxygen fugacity (oxidation) profiles of the DWPF pour spout in conjunction with the higher waste loadings. The DWPF liquidus model was developed to prevent volume crystallization of the melt pool at the normal melt pool temperatures, e.g. between 1050-1150°C, and at the normal oxygen fugacities experienced in waste glass melters, e.g. between $\log f_{O_2} = -2$ ($Fe^{+2}/\Sigma Fe=0.09$) and $\log f_{O_2} = -9$ ($Fe^{+2}/\Sigma Fe=0.33$). Operation of the SGM melter, specifically SGM Campaign 6, at waste loadings in excess of 38 wt%, e.g. in the range in which DWPF experienced severe pour spout crystallization, is achievable if the pour spout is well insulated and kept hot.

In the DWPF pour spout the glass flows up the riser, down the pour spout, and over the pour spout insert. During this path the following occurs:

- cooler temperatures are encountered, e.g. <1050°C which is below the liquidus of the glass being poured which initiates crystallization of spinel
- more oxidizing atmospheres (fugacities) are encountered, e.g. air $\log f_{O_2} = -0.68$ which enhances the kinetics of the crystallization of spinel relative to the reducing atmosphere of the melt pool ($\log f_{O_2} = -5.5$)
- cooler Inconel® 690 surfaces are contacted that act as heat sinks inducing surface crystallization instead of bulk or volume crystallization
- cooler Inconel® 690 surfaces are contacted that are themselves being oxidized due to exposure to air and these surfaces release $Cr_2O_3$, which can nucleate spinels

If the DWPF pour spout insert and upper pour spout bore are cooler than the liquidus temperature predicted by the DWPF Product Composition Control System (PCCS), e.g. a liquidus temperature of 987°C predicted for MFT 245 and a liquidus of 997°C predicted from the pour stream analysis, then surface nucleation of crystals on these cooler surfaces is more likely to occur. This is because a higher waste loaded melt is closer to its crystallization temperature when it exits the melter than a lower waste loaded melt. Thus, unless a higher waste loaded melt is moved through the cooler region very rapidly, the glass crystallizes instead of "undercooling" to an amorphous state. In other words, the riser temperature profile is too steep (the bore is not hot enough) which allows spinels to form at higher waste loadings because the cooling rate is not fast enough in this region.

This mechanism is supported by the analyses performed in this study. The mass balance of the pour spout insert samples based on the chemical analysis and the XRD identification of $NiFe_2O_4$ and $Cr_2O_3$, indicated that the sample was ~73 wt% glass, 16.4 wt% $NiFe_2O_4$, and 21 wt% $Cr_2O_3$. At the temperature of the pour spout insert, Inconel® 690 has been found to rapidly oxidize to form a protective chrome oxide layer. Ni-rich alloys such as Inconel® 690 oxidize to $NiCr_2O_4$ and NiO. This "free" NiO can further complex with the $Fe_2O_3$ in DWPF glass forming $NiFe_2O_4$ which depletes the Inconel® 690 in NiO leaving an enrichment in $Cr_2O_3$ as a scale which can act as nucleation sites for additional deposits.

The mass balance of the upper bore samples based on the chemical analysis and the XRD identification of $Ni(Cr,Fe)_2O_4$ indicated that the sample was 62 wt% glass, 7.7 wt% $NiCr_2O_4$ and 25.8 wt% $NiFe_2O_4$. Formation of such high concentrations of $NiCr_2O_4$ in this region may be related to the oxidation of Inconel® 690. Oxidation of Inconel® 690 can also form NiO which reacts with $Fe_2O_3$ in DWPF glass forming $NiFe_2O_4$. The presence of high concentrations of $NiCr_2O_4$ in the upper pour spout bore indicates that there is sufficient oxygen available in this region to cause such oxidation. Corrosion (oxidation) of Inconel® 690 in the DWPF riser, bore, and insert can be enhanced by the following:

- higher concentrations of $Fe_2O_3$ in DWPF glass at the higher waste loadings being processed where the $Fe_2O_3$ content could be acting as a diffusion driver for reaction with Ni being oxidized from the Inconel® 690

- higher concentrations of noble metals in SB2 accelerating Inconel® 690 corrosion

Knowing that the DWPF pour spout bore and insert regions are more oxidizing than the melt pool and not sufficiently hot enough allows higher waste loaded glasses to cool too slowly. In other words, the degree of undercooling is too great, and the surface nucleation of spinels on the inside of the upper bore, spout, and insert can occur. The surface nucleation of spinels in the cooler more oxidizing regions of the pour spout is further enhanced in oxidizing environments because the activation energy of spinel nucleation is more rapid (17.7 kcal/mole) than in reducing environments (2.9 kcal/mole). In addition, the oxidative corrosion of Inconel® 690 provides excess $Cr_2O_3$ nuclei that can act as heterogeneous nuclei for spinel growth.

The oxidative corrosion of Inconel® 690 and the insufficient heat in the pour spout mechanism is consistent with the operating history of the LSFM which had a pour spout temperature of ~1075°C, poured lower waste loaded glasses, and did not experience any pour spout pluggages.

The oxidative corrosion of Inconel® 690 and the insufficient heat in the pour spout mechanism is also consistent with the pour spout pluggages experienced during SGM-1 when the pour spout tip was 980°C. Once the SGM-1 pour spout was better insulated and the thermocouple locations redesigned, the SGM was able to pour glasses with calculated waste loadings up to ~42 wt%, e.g. SGM 6-6.

One other observation noted in this study was elevated $Cr_2O_3$ in the pour stream over that analyzed in the SME and MFT may indicate one of the following:

- analytic error
- K-3 refractory corrosion due to lack of MgO in the Frit 320 formulation although SB 2 contains sufficient MgO that this should not be a problem
- oxidation of the Inconel® 690 in the riser

Elevated $Cr_2O_3$ in the pour stream will raise the liquidus temperature of the glass and the nucleation frequency will be greater at higher undercoolings as discussed in Section 4.1.1.

The following recommendations are made based on the analyses performed in this study:

- Study the corrosion of Inconel® 690 in the presence of higher $Fe_2O_3$ containing (higher waste loaded glasses) in reduced melts, e.g. at an $Fe^{+2}/\Sigma Fe$ ratio of 0.2
- Study the corrosion of Inconel® 690 in the presence of noble metals at a $Fe^{+2}/\Sigma Fe$ ratio of 0.2
- Measure the temperature of the upper bore
  - initiate measures to increase the heat in the pour spout upper bore and insert region
- Measure the corrosivity of K-3 refractory under reduced conditions in the presence and absence of MgO in the frit

## TABLE OF CONTENTS

1.0 INTRODUCTION ..... 1

2.0 BACKGROUND ..... 3
2.1 Project 1941 Melter ..... 3
2.2 Small Cylindrical Melter (SCM) ..... 4
2.3 Large Slurry Fed Melter (LSFM) ..... 5
2.4 Scale Glass Melter (SGM) ..... 5
2.5 Integrated DWPF Melter System (IDMS) ..... 6
2.6 Pilot Scale Melter Waste Loadings and Predicted Liquidus Temperatures ..... 7

3.0 SAMPLE ANALYSES ..... 15
3.1 Visual Observation ..... 15
3.2 Elemental Analyses ..... 17
3.3 Noble Metal Analyses ..... 21
3.4 REDOX Analyses ..... 22
3.5 Glass Density Measurement ..... 23
3.6 Contained Scanning Electron Microscopy (CSEM) ..... 24
3.7 Contained X-ray Diffraction Analysis (CXRD) ..... 29

4.0 DISCUSSION ..... 32
4.1 Pour Stream Sample ..... 32
4.2 Pour Spout Insert Sample ..... 33
4.3 Upper Pour Spout Bore Sample ..... 34

5.0 POTENTIAL MECHANISMS FOR ACCUMULATION OF MELTER DEPOSITS IN THE DWPF POUR SPOUT ..... 35
5.1 Gradients in Temperature and Oxygen Fugacity ..... 35
5.1.1 Heat Sink Induced Crystallization ..... 36
5.1.2 Inconel® 690 Oxidation and Induced Crystallization ..... 41
5.2 Elevated $Cr_2O_3$ in the Pour Stream ..... 43

6.0 CONCLUSIONS ..... 44

7.0 RECOMMENDATIONS ..... 46

8.0 REFERENCES ..... 47

## TABLE OF FIGURES

Figure 1. Region of the upper pour stream bore from which the PC0031 sample was taken. Note deposits appear thicker on glass pour side. .....1

Figure 2. Region of the pour spout insert from which the PC0031 sample was taken. Note the heavy buildup of deposits. .....2

Figure 3. Comparison of the liquidus temperatures for various pilot scale melters calculated historically and with the newly implemented DWPF quasicrystalline model. .....13

Figure 4. Comparison of the liquidus temperatures and waste loadings for various pilot scale melters calculated with the newly implemented DWPF quasicrystalline model. .....14

Figure 5. From top to bottom, A) black and shiny pour stream sample PC0033, B) dark gray and matte insert sample PC0031, and C) upper pour spout bore sample PC0006. .....16

Figure 6 .Representative micrograph of the insert sample glass (PC0031), 500X in back scatter which makes high atomic element cations appear "lighter" than the remaining matrix. ..25

Figure 7. EDS spectrum of the bright coating (left hand side of sample) on the insert sample glass (PC0031). Sample is coated with Au and Pd to minimize charging. .....25

Figure 8. EDS spectrum of the right hand side of the grain of the insert sample glass (PC0031) exhibiting the coating in Figure 6. Sample is coated with Au and Pd to minimize charging. EDS spectra is typical of glass. .....26

Figure 9. EDS spectra of chromium and iron rich spinels in insert sample glass (PC0006). .....27

Figure 10. EDS spectra from the insert sample (PC0006) showing the composition of typical glass including the uranium component. .....28

Figure 11. CXRD spectra of two of the three pour stream samples analyzed (PC0033) showing that the pour stream does not contain any spinels or other crystals. .....30

Figure 12. CXRD spectra of the insert glass sample (PC0031). .....31

Figure 13. CXRD spectra of the upper pour stream bore sample (PC0006). .....32

Figure 14. Relationship between the glassy, liquid and solid states (from Reference 60). .....37

Figure 15 Comparison of the liquidus temperatures for various pilot scale melters compared to the samples analyzed in this study (solid black circles). .....39

Figure 16 Comparison of the liquidus temperatures and waste loading for various pilot scale melters compared to the samples analyzed in this study (solid black circles). .....40

Figure 17. Comparison of the calculated viscosities and waste loadings for various pilot scale melters compared to the samples analyzed in this study (solid black circles). ..... 41

Figure 18. Binary phase diagram at 1050°C demonstrating the phases that are formed upon oxidation of a Ni-Cr alloy like Inconel® 690 [78]. ..... 42

## TABLE OF TABLES

Table I. Savannah River Site Pilot Scale Melters Operated In Support of DWPF Design. ..... 7

Table II. Melt History of the Small Cyclindrical Melter, the Large Scale Melter System (LSFM), the Scale Glass Melter (SGM) and the Integrated DWPF Melter System (IDMS). ..... 8

Table III. Compositions of Glasses Processed in Various SRS Pilot Scale Melters. ..... 10

Table IV. Measured Compositions of the DWPF Melter #2 Samples Compared to SRTC Tank 40 Glass and DWPF SME Batch 245 and MFT Batch 245 (in Oxide Wt.%) ..... 20

Table V. Ratio of Major Components of the Pour Stream Sample to the Upper Pour Stream Bore Sample, to the Insert Sample, and to the SME 245 and MFT 245 Analyses. ..... 21

Table VI. Mass Balance for Samples Based on Data in Table IV. ..... 21

Table VII. Comparison of the Noble Metals (wt.%) of the SRTC Tank 40, Pour Stream, Upper Pour Spout Bore, and Insert Glasses. ..... 22

Table VIII. REDOX of Pour Stream (PC0033) Glass Prepared in the SRTC Shielded Cells. ..... 24

## LIST OF ACRONYMS

| | |
|---|---|
| ARG-1 | Approved Reference Material |
| CSEM | Contained Scanning Electron Microscopy |
| CXRD | Contained X-ray Diffraction |
| DWPF | Defense Waste Processing Facility |
| EDS | Energy Dispersive Spectroscopy |
| EMF | Electro-Motive Force |
| HAN | Hydroxyl Amine Nitrate |
| IC | Ion Chromatography |
| ICP-ES | Inductively Coupled Plasma – Emission Spectroscopy |
| ICP-MS | Inductively Coupled Plasma – Mass Spectroscopy |
| IDMS | Integrated DWPF Melter System |
| LSFM | Large Slurry Fed Melter |
| MA | Mixed Acid |
| MAR | Measurement Acceptable Region |
| MFT | Melter Feed Tank |
| PCCS | Product Composition Control System |
| PF | Peroxide Fusion |
| PHA | Precipitate Hydrolysis Aqueous |
| REDOX | REDuction/OXidation |
| SB-2 | Sludge Batch-2 |
| SCM | Small Cylindrical Melter |
| SGM | Scale Glass Melter |
| SME | Slurry Mix Evaporator |
| SRTC | Savannah River Technology Center |
| TDS | Technical Data Summary |

# CHARACTERIZATION OF DEFENSE WASTE PROCESSING FACILITY (DWPF) GLASS AND DEPOSIT SAMPLES FROM MELTER #2 (U)

**C.M. Jantzen, A.D. Cozzi, and N.E. Bibler**
**Savannah River Technology Center**
**Aiken, South Carolina 29808**

## 1.0 INTRODUCTION

Defense Waste Processing Facility (DWPF) Engineering requested characterization of three glass samples that were taken from Melter #2 after the waste loading had been increased, e.g. after the new liquidus model [1] had been implemented and after DWPF switched from processing with Frit 200 to Frit 320. These samples were taken after DWPF observed very rapid buildup of deposits in the upper spout bore and on the pour spout insert while processing high waste loading (~38 wt%) feedstock. Rapid deposition in these locations had not occurred prior to processing the high waste loaded feeds and stopped after waste loading was decreased.

The sample analyses performed included chemical composition, noble metals, crystal content, and REDuction/OXidation (REDOX) expressed as the $Fe^{+2}/\Sigma Fe$ ratio. The three glasses consisted of the following:

- a pour stream sample taken while filling canister S01859 during processing of Sludge Batch 2 (SB2),

- a sample that was scraped from the 2 inch upper pour spout bore (Figure 1) using a 1-7/8" diameter rotating drill bit,
  - the material had grown/accumulated at or just below the transition from the riser to the pour spout [2],
  - the sample had been taken from the bore while it was hot,

- a sample of glass adhering to a Melter #2 Type I insert (Figure 2) that had spalled from the interior of the insert after it had cooled [2].

The samples were taken on August 28, 2003. The glass being processed at that time corresponded to Slurry Mix Evaporator (SME) and Melter Feed Tank (MFT) batches 245, respectively. The samples had been taken after ~5 months operation of DWPF Melter #2.

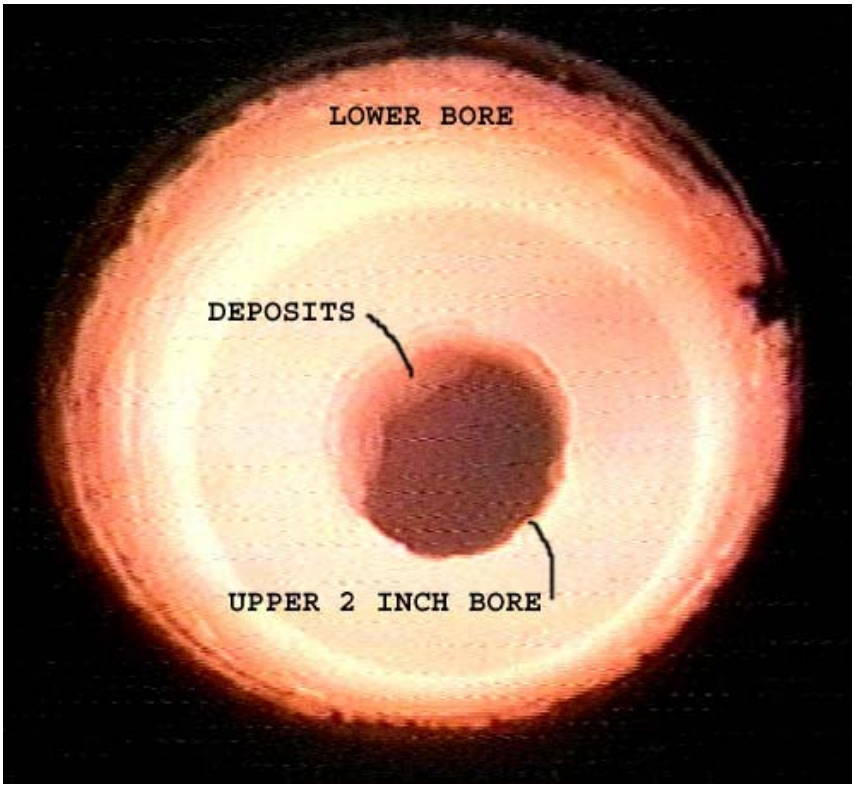


Figure 1. Region of the upper pour stream bore from which the PC0031 sample was taken. Note deposits appear thicker on glass pour side. This is not typical of normal operations.

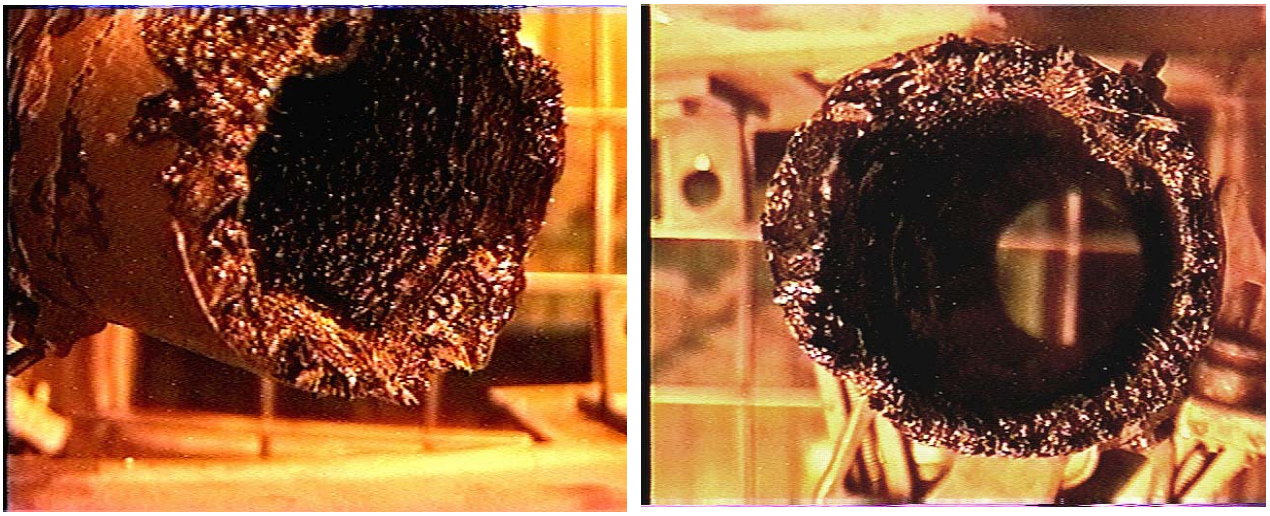

Figure 2. Region of the pour spout insert from which the PC0031 sample was taken. Note the heavy buildup of deposits. This is not the typical appearance of DWPF melter inserts during processing of lower waste loaded feeds.

## 2.0 BACKGROUND

The Savannah River Site has operated various pilot scale melters in support of the design of DWPF (Table I) since 1978. The scale of these melters is usually compared to DWPF based on the melt pool surface area in $ft^2$ and melt rate achieved which is also given in Table I. For reference the DWPF melt pool surface area is 28.26 $ft^2$ and the reference melt flux is 8 lbs/hr per $ft^2$ of melter surface area or ~228 lbs/hr. Some of these pilot scale melters experienced crystalline buildups on the floor of the melters and/or in the pour spout risers and nozzles. Details of these crystalline buildups, especially those involving the pour spout, are described below.

### 2.1 Project 1941 Melter

The 1941 melter was ~½ the DWPF melt pool surface area and was initially dry fed a calcine oxide sludge and later slurry fed. The melter produced 74 tons of simulated waste glass. During the dry calcine feeding a crystalline layer of ~7 inches thick formed [3]. This material formed primarily during a 58 day idle at 1050°C. Upon probing the melter after the idle period, the deposits on the bottom of the melter floor were determined to be very dense ("hard") and comprised 4" of spinel deposits [3]. A less dense spinel layer comprised the remaining 5 inches of deposits. When the 1941 large scale melter was shut down, it was dismantled to evaluate its service life [4]. Additional crystalline deposits up to approximately 1 inch thick were found to have formed on the walls of the melter and in the riser and nozzle.

The deposits on the walls of the 1941 melter were comprised of ~30 vol% spinel and were attributed to reaction of the refractory with the glass [4]. The crystalline deposits found in the riser and nozzle of the 1941 melter were found to have almost completely plugged the riser [4]. When enough crystalline material had accumulated to fill the bottom of the 1941 melter, the

deposits began to come out of the melter with the waste glass [4]. The large accumulations of three chemically distinct layers that eventually blocked the riser in the 1941 melter were attributed to the following:

- the bottom deposits, were composed of Cr enriched spinels, an unidentified silicate, and a glass matrix enriched in alumina – this was attributed to corrosion of the K-3 refractory

- the second layer was composed of spinels, a sodium calcium iron silicate similar in composition to acmite, a glassy matrix, and entrapped waste glass of a normal (not alumina enriched) composition

- the top layer was similar to the second layer but did not contain entrapped waste glass.

The deposition of the other layers was attributed to the low temperature idling of the melt pool at 1050°C for 58 days between Campaigns 3 and 4 and idling that occurred during conversion of the melter from calcine fed to slurry fed operation [3,4].

## 2.2 Small Cylindrical Melter (SCM)

The Small Cyclindrical Melter (SCM) had a melt pool surface of 1.3 $ft^2$ and was designed to test the performance of the various materials of construction when subjected to a variety of simulated waste and frit compositions [5]. It produced 24,511 pounds of glass in the first two campaigns which were dry powder feeds of simulated average (Technical Data Summary, TDS) sludge with either Frit 21B or Frit 211 (Table II). The third campaign began as dry fed TDS sludge and Frit 131 and produced 27,010 lbs of glass. The second part of the third campaign was slurry fed using TDS sludge and Frit 131and produced 11,359 lbs. of glass.

During Campaign 1 the drain valve was found to have insufficient power which did not allow initiation or maintenance of glass flow. Draining was hindered by a plug of devitrified/crystallized glass containing primarily $Li_2SiO_3$ nucleated by $TiO_2$ and the drain valve was redesigned [6]. The riser was lined with K-3 refractory rather than Inconel® 690 as in the DWPF design and showed accelerated wear. During SCM Campaign 1 [6] and Campaign 2 [7], the most accelerated melt flux tested, it was determined that the K-3 refractory lining the riser was dissolving due to the high molten glass velocities. In addition, during Campaign 1 severe corrosion of the Inconel® 690 was observed in hot oxidizing environments and due to sulfidization [6]. During Campaign 2 lumps of unmelted feed material were observed in the glass pour stream [5] when the melter was overfed. Additional studies performed by Routt, Plodinec, and Porter in the SCM demonstrated that spinel accumulated on the melter bottom when the melt pool temperature was lowered from 1150°C to 1050°C [7].

### 2.3 Large Slurry Fed Melter (LSFM)

The LSFM produced over 240 tons of simulated defense waste (based on Frits 131 and 165 and a reducing formated flowsheet) over a two year period of operation [8]. There were no riser or pour spout pluggages reported. The riser temperatures were reported to be in the range of 1125°C ± 10°C and the pour spout temperatures were reported to be 1075°C ± 10°C during the 5$^{th}$ Campaign [9]. Only 1/16 to 1/2 inch of crystalline deposits were observed on the bottom of the SRL Large Slurry Fed Melter (LSFM) melter when it was bottom drained [8].

### 2.4 Scale Glass Melter (SGM)

The Scale Glass Melter (SGM) produced ~90 tons of glass in two years based on Frits 165, 168, and 200 and a reducing (formic acid) flowsheet (Table II). Crystalline deposits were not found in the SGM when the melter bottom was probed, e.g. after the 5th melter Campaign (SGM-5) [10]. When the SGM was bottom drained after the 9th Campaign (SGM-9) no significant accumulations of deposits were observed [11]. The lack of crystal formation in the large scale LSFM [8] and in the SGM [10] melters has been attributed [10] to better melter design, slurry feeding rather than pre-calcining, control of rheology and REDuction/OXidation (REDOX) by formic acid addition, and more solubilizing frit compositions.

The in-situ formation of crystalline deposits in the SGM melter pour spout, similar to those experienced by DWPF Melter #2, were experienced during the SGM-1 campaign due to a cool pour spout tip [12], e.g. 980°C on the glass contact side (Pour Spout Thermocouple PS3) near the disengagement point, 1040°C closer to the pour spout bore (Pour Spout Thermocouple PS2) and 600°C on the opposite side (Pour Spout Thermocouple PS1) during steady state pouring [13]. Crystallization of these deposits resulted in frequent channel pluggages and reduced production rate (~50%). Pluggages formed in the pour spout discharge tube on 10 different occasions. The pluggages were composed of visibly crystallized (i.e. devitrified) glass. Batch pouring aggravated plugging; pluggages appeared to become worse as the length of time between pours increased.

Characterization of the size, composition, and volume fraction of the crystallized (devitrified) phases in the SGM-1 pour spout were used to interpret the thermal history of the glass [14]. The identification of acmite crystals indicated that the affected sections of the pour spout were as cool as ~700°C while the thermocouples indicated that this region was hotter. The lack of spinel formation which normally occurs between 750-1025°C [15,16,17,18,19], confirmed that the pour spout was very cool (<750°C). The size of the crystals indicated that the crystals had formed in the pour spout at these low temperatures over long time periods.

This pour spout pluggage and associated interpretation of the thermal history [14] led to a redesign of the pour spout, e.g. better insulation and relocation of the thermocouples to accurately profile pour spout temperatures. After this redesign, the SGM did not experience severe pour spout pluggages.

## 2.5 Integrated DWPF Melter System (IDMS)

The IDMS melter had poured ~46, 400 pounds of glass based on Frits 165 and 202 with a reducing flowsheet and ~45,200 pounds of glass based on Frit 202 with various oxidizing nitric acid flowsheets (see Table II) [20]after seven years of continuous operation. The IDMS did not experience any pour spout pluggages even when the measured pour spout tip temperature was 974°C [21] . An auxiliary heater was tested during the 4$^{th}$ Campaign of the IDMS which increased the pour spout tip temperature to 1010°C [13].

The IDMS melter had accumulated approximately 12 inches of glassy and crystalline deposits on the melter bottom [20]. Due to a bottom drain failure, the IDMS melter was drained by pulling a vacuum on the pour spout. Therefore, some portion of the 12 inches of glassy and crystalline deposits analyzed were due to solidification of the glass that remained in the melter and could not be drained. The IDMS deposits were analyzed as a function of depth by taking core drilled samples. The samples were enriched in $Cr_2O_3$ (~1 wt%) and NiO (1.5-2.0 wt%) over the amounts of these constituents contained in the glasses processed. These melter floor deposits contained between 3.2-8.5 wt% spinel [20] not the ≥30 volume% spinel found in the 1941 melter, SCM and PNNL melters. Deposits embedded in the floor of the IDMS melter where the glass had reacted with the refractory over the 7 year operation of this melter were found to contain 9.2-18.68 wt% $Cr_2O_3$ and ~1 wt% NiO as 27-66 wt% spinel [20, 22].

Table I. Savannah River Site Pilot Scale Melters Operated In Support of DWPF Design.

| Melter Designation | Melt Pool Surface Area ($ft^2$) | Reference Pour Rate ($lbs/hr(ft)^2$)* | Year of Initial Operation | Pour Spout/Riser Pluggages | Crystal Buildup on Floor of Melter During Operation |
|---|---|---|---|---|---|
| Large Scale Project 1941 Melter | 12 | 96 | 1978-1979 | Yes | 9” |
| Small Cylindrical Melter (SCM) | 1.3 | 10.4 | 1979-1982 | No | Several inches per campaign |
| Large Slurry Fed Melter (LSFM) | 12 | 96 | 1982-1985 | No | 1/16-1/2” |
| Scale Glass Melter (SGM) | 12.6 | 100.8 | 1986-1988 | Yes | None |
| Integrated DWPF Melter System (IDMS) | 3.14 | 25.12 | 1988-1994 | No | None |

* DWPF Design Basis of 228 lbs/hr or $8lbs/hr(ft)^2$ times melt pool surface area ($ft^2$)

### 2.6 Pilot Scale Melter Waste Loadings and Predicted Liquidus Temperatures

The glass composition data from the SCM-2, the LSFM, and the SGM was compiled into a database (see Table III). Compositional data for the LSFM and SCM-2 was compiled from analyzed feed and frit compositions. Compositional data for the SGM campaigns was from analyzed glasses from taken from full sized canisters. Compositional data for the Project 1941 melter could not be found. The analyzed glass composition data from the IDMS and from the DWPF Qualification runs was available but the glass analyses from these melter campaigns was suspect due to $Cr_2O_3$ contamination from the grinders used [23]. Since $Cr_2O_3$ content has a large impact on the liquidus temperature calculated from the quasicrystalline model [1] this data was not included in comparison of pilot scale melters and DWPF operational history, e.g. predicted liquidus and waste loading.

Table II. Melt History of the Small Cyclindrical Melter, the Large Scale Melter System (LSFM), the Scale Glass Melter (SGM) and the Integrated DWPF Melter System (IDMS).

| Melter Campaign | Frit/Sludge/Flow sheet | Lbs. of Glass Produced | Reference |
|---|---|---|---|
| SCM1-1 | Frit 21B + Frit 211/TDS Average Sludge Only/Dry Fed | 6000 | 5 |
| SCM1-2 | Frit 211/TDS Average Sludge Only/Dry Fed | 18,511 | 5 |
| SCM1-3 | Frit 131/TDS Average Sludge Only/ Dry Fed<br>Frit 131/TDS Average Sludge Only/Slurry Fed | 27,010<br>11,359 | 5 |
| LSFM-1 | Black Startup Frit + Frit 131/Stage I Average Sludge/Slurry Fed | 2,750 | 24 |
| LSFM-2 | Frit 131/Stage I Average Sludge/Slurry Fed with Formate | 4,500 | 25 |
| LSFM-3 | Frit 131/Stage I Average Sludge/Slurry Fed with Formate | 11,025 | 26 |
| LSFM-4 | Frit 131/Stage 1 Average Sludge Only/Slurry Fed with Formate | ~11,000 | 27 |
| LSFM-5 | Frit 131/ Stage 1 Average Sludge Only/Slurry Fed with Formate | >35,000 | 9 |
| LSFM-6 | Frit 165/ Stage 1 Average Sludge Only/Slurry Fed with Formate | 14,000 | 28 |
| LSFM-7 | Frit 165/ Stage 1 Average Sludge Only/Slurry Fed with Formate | 17,622 | 29 |
| LSFM-8 | Frit 165/ Stage 1 Average Sludge Only/Slurry Fed with Formate | 32,570 | 30 |
| LSFM-9 | Frit 131 and 165/ Stage 1Average Sludge Only/Slurry Fed with Formate | 158,760 | 31 |
| LSFM-10 | Frit 165 and Bickford Average Sludge*/Slurry Fed with Formate | 26,605 | 32 |
| SGM-1 | F165/Average/Sludge Only/ Slurry Fed | 21,000 | 12 |
| SGM-2+3 | F200/Average/Coupled PHA/ Slurry Fed | 20,700 | 12 |
| SGM-4+5 | F168/Average/ Sludge Only/ Slurry Fed | 29,300 | 12, 33 |
| SGM-6+7 | F200/Average/Coupled HAN PHA<br>F200/F168/Average/Coupled HAN PHA | 51,500 | 34 |
| SGM-8 | 165 Black Frit | 37,000 | 35 |
| SGM-9 | F200/Average/Coupled HAN PHA + Organics | 28,551 | 36 |
| SGM-10 | F168/Average/Coupled PHA + Organics | 7,623 | 36 |
| IDMS Startup | DWPF Startup Frit | 200 | 21 |
| IDMS Base | F165/Average/Sludge Only | 7390 | 21 |
| PHA #1,2,3 | F202/Batch 1 Sludge/Coupled HAN PHA | 15,052 | 37 |
| IDMS Hg Runs | F202/Batch 1 Sludge/Coupled with PHA | 14,123 | 38 |
| IDMS Blend 1 | F202/Blend 1 Sludge with Noble Metals/Coupled with PHA | 2,809 | 39 |
| IDMS Blend 2 | F202/Blend 2 Sludge/Coupled with PHA | 5,014 | 39 |
| IDMS Blend 3 | F202/Blend 3 Sludge/Coupled PHA | 1,774 | 40 |
| IDMS HM-1 | F202/HM Sludge/Coupled with PHA + NaNO3 | 2,977 | 40 |
| IDMS HM-2 | F202/HM Sludge/Coupled PHA | 2,739 | 41 |
| IDMS HM-3 | F202/HM Sludge/Coupled PHA | 4,048 | 41 |
| IDMS PX-2 | F202/Purex Sludge/Coupled PHA | 3,120 | 41 |
| IDMS PX-1 | F202/Purex Sludge/Coupled PHA | 4,073 | 41 |
| IDMS Hanford | Hanford Waste + Frit + Nitric Acid | 7,951 | 42 |
| IDMS HM-4 | F202/HM Sludge/Nitric Acid + HAN | 4,355 | 41 |
| IDMS PX-3 | F202/Purex Sludge/Coupled HAN | 5,073 | 41 |
| IDMS PX-4 | F202/Purex Sludge/Nitric Acid + Late Wash PHA | 4,850 | 41 |
| IDMS PX-5 | F202/Purex Sludge/Nitric Acid + Late Wash PHA | 4,075 | 41 |
| IDMS PX-6 | F202/Purex Sludge/Nitric Acid + Late Wash PHA | 1,943 | 43 |

* lower in $SiO_2$ than TDS Average or Stage 1 Average simulated sludge

The data in Table III was used to calculate the DWPF liquidus temperature from the DWPF historic liquidus model [44], the DWPF liquidus temperature from the newly implemented quasicrystalline model [1], and the waste loading achieved based on the $Li_2O$ content of the frit [45], the latter being the method currently used by DWPF to calculate waste loading. A comparison of the predicted liquidus temperature model calculated two different ways is shown in Figure 3 while the comparison of the quasicrystalline liquidus temperature to waste loading is shown in Figure 3. The ordinary least squares equation of best fit for the data shown in Figure 3 is

Equation 1 Quasicrystalline Liquidus (°C) = -590.476 + 1.5276 (Historic Liquidus in °C).

with an adjusted $R^2$ of 0.82 and a Root Mean Square Error of 34.58. Figure 3 shows the following:

- there is a linear correlation between the historic and quasicrystalline liquidus models (see Equation 1)
- there is ~ a 36°C offset in the historic liquidus (1050°C) and the corresponding quasicrystalline liquidus (1013°C) at the DWPF liquidus temperature limit of 1050°C
- pilot scale melters such as the LSFM operated at lower liquidus values than the other pilot scale melters, e.g. SGM and SCM-2

A combination of the data displayed in Figure 3, the data given in Table III, and the operating experiences summarized in Sections 2.2 to 2.4 shows the following:

- the lower liquidus values experienced during the LSFM campaigns was associated with lower waste loadings in the range of 20-32 wt% when calculated from the $Li_2O$ values in the frits that were used
- the scale glass melter (SGM-6), which had a DWPF prototypic pour spout and ran reducing flow sheets, ran some very high waste loadings (up to 42 wt%) and no pour spout pluggages were experienced once the pour spout was insulated and the thermocouples relocated after the SGM-1 campaign.

Table III. Compositions of Glasses Processed in Various SRS Pilot Scale Melters.

| Glass ID | Ref | $Al_2O_3$ | $B_2O_3$ | CaO | $Cr_2O_3$ | CuO | $Fe_2O_3$ | $K_2O$ | $Li_2O$ | MgO | MnO | $Na_2O$ | NiO | $SiO_2$ | $TiO_2$ | $ZrO_2$ | Sum of Oxides | Old $T_L$ (°C) | New $T_L$ (°C) | Visc. (poise) | $Li_2O$ in frit | Waste Loading $Li_2O$ |
|---|---|---|---|---|---|---|---|---|---|---|---|---|---|---|---|---|---|---|---|---|---|---|
| SGM 6-3 2B-1 | Canister 6-3 | 4.03 | 9.34 | 1.15 | 0.04 | 0.00 | 13.60 | 2.07 | 2.92 | 1.00 | 1.89 | 12.71 | 1.22 | 48.07 | 0.55 | 0.00 | 98.58 | 1039 | 973 | 48 | 4.39 | 32.56 |
| SGM 6-3 2T-1 | Canister 6-3 | 4.30 | 10.02 | 1.51 | 0.10 | 0.00 | 13.02 | 2.17 | 2.95 | 1.16 | 0.20 | 12.93 | 1.08 | 47.40 | 0.69 | 0.09 | 97.61 | 1035 | 974 | 45 | 4.39 | 31.08 |
| SGM 6-3 2T-2 | Canister 6-3 | 4.25 | 10.14 | 1.50 | 0.09 | 0.00 | 13.23 | 2.19 | 2.97 | 1.18 | 0.20 | 12.86 | 1.11 | 46.61 | 0.70 | 0.08 | 97.12 | 1043 | 978 | 41 | 4.39 | 30.3 |
| SGM 6-3 2T-3 | Canister 6-3 | 4.28 | 10.03 | 1.49 | 0.11 | 0.00 | 12.87 | 2.25 | 2.94 | 1.18 | 0.20 | 12.85 | 1.08 | 46.35 | 0.69 | 0.09 | 96.41 | 1038 | 978 | 42 | 4.39 | 30.48 |
| SGM 6-3 2T-4 | Canister 6-3 | 4.26 | 10.09 | 1.51 | 0.09 | 0.00 | 12.80 | 2.22 | 2.96 | 1.19 | 0.20 | 12.56 | 1.26 | 46.54 | 0.70 | 0.09 | 96.46 | 1036 | 990 | 44 | 4.39 | 30.21 |
| SGM 6-3 3-B | Canister 6-3 | 4.29 | 9.05 | 1.40 | 0.12 | 0.00 | 13.34 | 2.49 | 2.78 | 1.10 | 1.81 | 12.31 | 1.08 | 44.71 | 0.65 | 0.00 | 95.12 | 1057 | 1009 | 43 | 4.39 | 33.51 |
| SGM 6-3 3-T | Canister 6-3 | 4.25 | 10.08 | 1.49 | 0.10 | 0.00 | 13.44 | 2.34 | 2.91 | 1.20 | 0.19 | 12.90 | 1.39 | 46.40 | 0.72 | 0.06 | 97.46 | 1048 | 1004 | 41 | 4.39 | 31.98 |
| SGM6-3 4B-1 | Canister 6-3 | 4.25 | 9.02 | 1.37 | 0.12 | 0.00 | 13.37 | 2.10 | 2.73 | 1.11 | 1.78 | 12.50 | 1.07 | 45.18 | 0.67 | 0.00 | 95.26 | 1054 | 1005 | 44 | 4.39 | 34.63 |
| SGM6-3 4T-2 | Canister 6-3 | 4.19 | 9.49 | 1.19 | 0.02 | 0.00 | 14.01 | 2.43 | 2.84 | 1.19 | 1.94 | 12.83 | 1.22 | 49.65 | 0.66 | 0.00 | 101.67 | 1039 | 977 | 54 | 4.39 | 36.29 |
| SGM6-3 4T-3 | Canister 6-3 | 4.16 | 9.80 | 1.44 | 0.10 | 0.00 | 12.76 | 2.28 | 2.79 | 1.18 | 1.82 | 12.07 | 1.12 | 45.57 | 0.72 | 0.04 | 95.84 | 1040 | 1000 | 47 | 4.39 | 33.72 |
| SGM6-3 4T-4 | Canister 6-3 | 4.25 | 9.92 | 1.46 | 0.09 | 0.00 | 12.77 | 2.20 | 2.83 | 1.20 | 1.86 | 11.82 | 1.25 | 45.73 | 0.73 | 0.04 | 96.16 | 1040 | 1017 | 49 | 4.39 | 32.92 |
| SGM6-3 5B-1 | Canister 6-3 | 4.40 | 9.18 | 1.40 | 0.13 | 0.00 | 13.84 | 2.32 | 2.71 | 1.16 | 1.90 | 12.33 | 1.08 | 46.25 | 0.72 | 0.00 | 97.43 | 1058 | 1023 | 49 | 4.39 | 36.59 |
| SGM 6-6 IT-1 | Canister 6-3 | 4.17 | 8.78 | 1.15 | 0.04 | 0.00 | 13.14 | 2.84 | 2.50 | 1.18 | 1.92 | 13.18 | 1.07 | 47.25 | 0.71 | 0.00 | 97.93 | 1037 | 956 | 52 | 4.39 | 41.92 |
| SGM6-6 2B-1 | Canister 6-3 | 4.08 | 8.92 | 1.20 | 0.02 | 0.00 | 13.14 | 2.58 | 2.56 | 1.19 | 1.89 | 12.48 | 1.04 | 48.13 | 0.72 | 0.00 | 97.96 | 1032 | 962 | 59 | 4.39 | 40.43 |
| SGM6-6 2T-3 | Canister 6-3 | 4.17 | 9.03 | 1.18 | 0.03 | 0.00 | 13.38 | 2.58 | 2.57 | 1.19 | 1.84 | 12.46 | 1.11 | 47.07 | 0.71 | 0.00 | 97.31 | 1042 | 978 | 54 | 4.39 | 39.79 |
| SGM 6-6 2T-4 | Canister 6-3 | 4.19 | 9.01 | 1.18 | 0.03 | 0.00 | 13.49 | 2.54 | 2.57 | 1.20 | 1.84 | 11.47 | 1.12 | 46.98 | 0.71 | 0.00 | 96.33 | 1045 | 1004 | 62 | 4.39 | 39.33 |
| SGM 6-6 3B | Canister 6-3 | 3.99 | 8.75 | 1.16 | 0.03 | 0.00 | 12.91 | 2.73 | 2.50 | 1.14 | 1.69 | 12.86 | 1.05 | 46.38 | 0.68 | 0.00 | 95.88 | 1036 | 952 | 51 | 4.39 | 40.68 |
| SGM 6-6 3T-1 | Canister 6-3 | 4.41 | 9.44 | 0.70 | 0.03 | 0.00 | 14.08 | 2.69 | 2.70 | 1.26 | 1.98 | 12.77 | 1.12 | 49.38 | 0.75 | 0.00 | 101.29 | 1043 | 983 | 56 | 4.39 | 39.35 |
| SGM 6-6 4T-1 | Canister 6-3 | 4.24 | 9.20 | 1.27 | 0.03 | 0.00 | 13.72 | 2.64 | 2.63 | 1.20 | 1.87 | 12.94 | 1.21 | 48.73 | 0.73 | 0.00 | 100.40 | 1040 | 978 | 55 | 4.39 | 40.42 |
| SGM 6-6 4T-2 | Canister 6-3 | 4.71 | 8.74 | 1.09 | 0.03 | 0.00 | 13.33 | 2.72 | 2.45 | 1.04 | 1.80 | 12.79 | 1.12 | 46.32 | 0.69 | 0.00 | 96.82 | 1050 | 979 | 54 | 4.39 | 42.32 |
| SGM 6-6 4T-4 | Canister 6-3 | 4.06 | 8.71 | 1.16 | 0.04 | 0.00 | 13.28 | 2.61 | 2.47 | 1.15 | 1.79 | 12.40 | 1.21 | 45.97 | 0.69 | 0.00 | 95.53 | 1046 | 987 | 52 | 4.39 | 41.08 |
| SGM 6-6 3A | Canister 6-3 | 4.40 | 9.18 | 1.37 | 0.13 | 0.00 | 13.35 | 2.37 | 2.73 | 1.14 | 1.90 | 12.21 | 1.03 | 46.51 | 0.72 | 0.00 | 97.05 | 1047 | 1013 | 52 | 4.39 | 35.84 |
| SGM 6-4A | Canister 6-3 | 4.29 | 8.92 | 1.29 | 0.12 | 0.00 | 13.14 | 2.52 | 2.60 | 1.16 | 1.85 | 12.60 | 0.98 | 45.67 | 0.75 | 0.00 | 95.89 | 1047 | 992 | 48 | 4.39 | 38.13 |
| SGM 6-4B | Canister 6-3 | 4.50 | 9.05 | 1.30 | 0.18 | 0.00 | 13.60 | 2.64 | 2.63 | 1.16 | 1.77 | 13.05 | 1.02 | 45.89 | 0.75 | 0.00 | 97.52 | 1056 | 1014 | 45 | 4.39 | 38.66 |
| SGM 6-6A | Canister 6-3 | 4.48 | 8.98 | 1.29 | 0.13 | 0.00 | 13.63 | 2.77 | 2.56 | 1.18 | 1.89 | 12.95 | 1.00 | 45.27 | 0.78 | 0.00 | 96.91 | 1061 | 1003 | 44 | 4.39 | 39.79 |
| SGM 6-3 B-2 | Canister 6-3 | 4.35 | 9.56 | 1.36 | 0.12 | 0.00 | 13.81 | 2.01 | 3.08 | 1.02 | 2.07 | 12.48 | 1.16 | 46.17 | 0.57 | 0.00 | 97.75 | 1057 | 1009 | 41 | 4.39 | 28.27 |
| SGM 6-3 B-2B1B | Canister 6-3 | 4.27 | 9.15 | 1.25 | 0.17 | 0.00 | 13.74 | 2.52 | 2.73 | 0.95 | 1.96 | 12.70 | 1.08 | 46.32 | 0.72 | 0.00 | 97.54 | 1054 | 1015 | 46 | 4.39 | 36.16 |
| SGM 6-6 4B | Canister 6-3 | 4.48 | 8.98 | 1.39 | 0.12 | 0.00 | 13.63 | 2.63 | 2.52 | 1.19 | 1.92 | 12.82 | 1.11 | 45.63 | 0.78 | 0.00 | 97.19 | 1058 | 1011 | 47 | 4.39 | 40.98 |
| SGM 6-6 5B-1 | Canister 6-3 | 4.46 | 8.95 | 1.37 | 0.12 | 0.00 | 13.55 | 2.76 | 2.52 | 1.16 | 1.94 | 12.93 | 1.09 | 45.14 | 0.78 | 0.00 | 96.77 | 1060 | 1005 | 45 | 4.39 | 40.72 |
| SGM 6-3 A-2 | Canister 6-3 | 4.48 | 9.60 | 1.36 | 0.13 | 0.00 | 13.91 | 2.45 | 2.71 | 1.14 | 1.98 | 13.01 | 0.99 | 47.07 | 0.73 | 0.00 | 99.55 | 1054 | 1000 | 46 | 4.39 | 37.94 |
| SGM 7-1 | Canister 7-1 | 3.96 | 10.24 | 1.34 | 0.13 | 0.00 | 12.12 | 2.40 | 3.04 | 1.11 | 1.65 | 12.75 | 0.98 | 46.19 | 0.43 | 0.05 | 96.40 | 1023 | 959 | 41 | 5 | 37.03 |

| Glass ID | Ref | $Al_2O_3$ | $B_2O_3$ | CaO | $Cr_2O_3$ | CuO | $Fe_2O_3$ | $K_2O$ | $Li_2O$ | MgO | MnO | $Na_2O$ | NiO | $SiO_2$ | $TiO_2$ | $ZrO_2$ | Sum of Oxides | Old $T_L$ (°C) | New $T_L$ (°C) | Visc. (poise) | $Li_2O$ in frit | Waste Loading $Li_2O$ |
|---|---|---|---|---|---|---|---|---|---|---|---|---|---|---|---|---|---|---|---|---|---|---|
| SGM 7-2B | Canister 7-2 | 3.65 | 10.63 | 1.30 | 0.13 | 0.00 | 11.31 | 2.24 | 3.16 | 1.10 | 1.70 | 12.46 | 0.94 | 46.87 | 0.32 | 0.15 | 95.95 | 1003 | 938 | 43 | 5 | 34.05 |
| SGM 7-3 | Canister 7-3 | 3.74 | 10.85 | 1.25 | 0.12 | 0.00 | 11.42 | 2.43 | 3.27 | 1.13 | 1.65 | 11.73 | 0.90 | 48.13 | 0.30 | 0.15 | 97.08 | 1000 | 947 | 50 | 5 | 32.59 |
| SGM 7-4 | Canister 7-4 | 3.28 | 10.87 | 1.05 | 0.20 | 0.00 | 12.46 | 2.36 | 3.26 | 1.04 | 1.52 | 12.09 | 1.16 | 50.38 | 0.22 | 0.55 | 100.44 | 1004 | 1001 | 52 | 5 | 35.19 |
| SGM 7-4 #2 | Canister 7-4 | 3.72 | 11.17 | 1.34 | 0.12 | 0.00 | 11.85 | 2.49 | 3.36 | 1.14 | 1.77 | 11.98 | 0.92 | 48.88 | 0.32 | 0.16 | 99.23 | 1003 | 946 | 48 | 5 | 32.32 |
| SGM 7-4 #3 | Canister 7-4 | 3.67 | 10.98 | 1.33 | 0.12 | 0.00 | 11.62 | 2.47 | 3.32 | 1.13 | 1.67 | 12.33 | 0.92 | 48.67 | 0.32 | 0.15 | 98.67 | 1000 | 933 | 46 | 5 | 32.81 |
| SGM 7-5 #4 | Canister 7-5 | 3.13 | 10.40 | 0.98 | 0.03 | 0.00 | 11.28 | 2.46 | 3.12 | 1.03 | 1.43 | 12.66 | 1.11 | 48.71 | 0.21 | 0.06 | 96.60 | 991 | 890 | 48 | 5 | 35.47 |
| SGM 7-5 | Canister 7-5 | 3.91 | 10.88 | 1.30 | 0.15 | 0.00 | 11.75 | 2.46 | 3.27 | 1.11 | 1.74 | 12.24 | 0.92 | 48.54 | 0.30 | 0.19 | 98.76 | 1004 | 956 | 48 | 5 | 33.74 |
| SGM 7-5 #7 | Canister 7-5 | 3.70 | 10.76 | 1.27 | 0.13 | 0.00 | 11.64 | 2.47 | 3.23 | 1.11 | 1.67 | 11.90 | 0.90 | 47.39 | 0.28 | 0.18 | 96.63 | 1007 | 953 | 47 | 5 | 33.17 |
| SGM 7-8 2B-2 | Canister 7-8 | 3.91 | 11.06 | 1.32 | 0.20 | 0.00 | 11.53 | 2.43 | 3.39 | 1.17 | 2.02 | 11.74 | 0.91 | 46.65 | 0.30 | 0.28 | 96.91 | 1010 | 983 | 43 | 5 | 30.08 |
| SGM 7-8 3B-2 | Canister 7-8 | 3.90 | 10.96 | 1.32 | 0.18 | 0.00 | 11.37 | 2.42 | 3.33 | 1.16 | 2.02 | 11.82 | 0.91 | 46.36 | 0.30 | 0.26 | 96.32 | 1008 | 973 | 43 | 5 | 30.77 |
| SGM 7-8 3B-3 | Canister 7-8 | 3.99 | 11.04 | 1.47 | 0.18 | 0.00 | 11.46 | 2.36 | 3.37 | 1.18 | 2.05 | 11.46 | 0.92 | 47.38 | 0.31 | 0.27 | 97.42 | 1005 | 985 | 48 | 5 | 30.89 |
| SGM 7-8 3B-5 | Canister 7-8 | 3.94 | 11.04 | 1.34 | 0.17 | 0.00 | 11.66 | 2.42 | 3.37 | 1.16 | 2.04 | 11.77 | 0.91 | 46.99 | 0.30 | 0.27 | 97.36 | 1011 | 975 | 44 | 5 | 30.71 |
| SGM 7-8 1T-2 | Canister 7-8 | 3.91 | 10.97 | 1.51 | 0.16 | 0.00 | 11.50 | 2.66 | 3.36 | 1.19 | 2.00 | 11.30 | 0.89 | 46.91 | 0.30 | 0.28 | 96.93 | 1008 | 980 | 48 | 5 | 30.72 |
| SGM 7-8 1T-3 | Canister 7-8 | 3.94 | 11.06 | 1.31 | 0.17 | 0.00 | 11.54 | 2.63 | 3.38 | 1.16 | 2.02 | 10.43 | 0.90 | 46.96 | 0.30 | 0.27 | 96.08 | 1009 | 1005 | 54 | 5 | 29.56 |
| SGM 7-8 1T-5 | Canister 7-8 | 3.74 | 11.91 | 1.42 | 0.10 | 0.00 | 11.45 | 2.18 | 3.50 | 1.19 | 1.59 | 11.47 | 0.93 | 50.13 | 0.32 | 0.22 | 100.16 | 991 | 946 | 53 | 5 | 30.15 |
| SGM 7-8 2T-1 | Canister 7-8 | 3.84 | 11.89 | 1.42 | 0.10 | 0.00 | 11.69 | 2.00 | 3.46 | 1.18 | 1.56 | 11.16 | 1.13 | 49.88 | 0.32 | 0.22 | 99.85 | 997 | 984 | 55 | 5 | 30.76 |
| SGM 7-8 2T-2 | Canister 7-8 | 3.68 | 11.83 | 1.42 | 0.10 | 0.00 | 11.39 | 2.31 | 3.43 | 1.17 | 1.54 | 11.85 | 0.88 | 49.74 | 0.31 | 0.22 | 99.86 | 992 | 932 | 50 | 5 | 31.41 |
| SGM 7-8 2T-3 | Canister 7-8 | 3.59 | 11.60 | 1.38 | 0.10 | 0.00 | 11.13 | 2.20 | 3.35 | 1.15 | 1.50 | 11.61 | 0.94 | 48.39 | 0.31 | 0.21 | 97.45 | 993 | 939 | 49 | 5 | 31.3 |
| SGM 7-8 3T-3 | Canister 7-8 | 3.78 | 11.75 | 1.47 | 0.10 | 0.00 | 11.82 | 2.35 | 3.34 | 1.15 | 1.64 | 11.39 | 1.18 | 47.77 | 0.32 | 0.21 | 98.28 | 1008 | 984 | 47 | 5 | 31.99 |
| SGM 7-8 3T-4 | Canister 7-8 | 3.80 | 11.63 | 1.61 | 0.10 | 0.00 | 11.83 | 2.51 | 3.32 | 1.15 | 1.71 | 10.92 | 1.16 | 48.67 | 0.32 | 0.22 | 98.94 | 1005 | 992 | 54 | 5 | 32.93 |
| SGM 7-8 3T-5 | Canister 7-8 | 3.72 | 11.63 | 1.41 | 0.09 | 0.00 | 11.56 | 2.29 | 3.33 | 1.13 | 1.59 | 11.49 | 1.04 | 47.44 | 0.32 | 0.21 | 97.24 | 1005 | 961 | 46 | 5 | 31.53 |
| SGM8 8/27/97 | 35 | 3.91 | 6.73 | 2.00 | 0.09 | 0.00 | 13.64 | 0.42 | 3.49 | 0.83 | 2.23 | 12.25 | 1.17 | 48.99 | 0.13 | 0.68 | 96.56 | 1034 | 999 | 55 | 4.94 | 26.9 |
| SGM8 8/28/97 | 35 | 3.89 | 6.63 | 2.39 | 0.07 | 0.00 | 13.87 | 0.30 | 3.36 | 0.75 | 2.41 | 12.52 | 1.21 | 48.35 | 0.15 | 0.76 | 96.67 | 1042 | 996 | 52 | 4.94 | 29.68 |
| SGM8 8/29/97 | 35 | 3.84 | 6.60 | 2.25 | 0.06 | 0.00 | 14.20 | 0.23 | 3.42 | 0.73 | 2.35 | 11.07 | 1.16 | 48.78 | 0.12 | 0.76 | 95.56 | 1044 | 1027 | 63 | 4.94 | 27.51 |
| SGM8 8/29/97 | 35 | 3.82 | 6.38 | 2.07 | 0.06 | 0.00 | 14.30 | 0.22 | 3.44 | 0.73 | 2.21 | 12.04 | 1.17 | 48.35 | 0.12 | 0.74 | 95.64 | 1048 | 1005 | 53 | 4.94 | 27.1 |
| SGM8 8/30/97 | 35 | 3.91 | 6.41 | 2.13 | 0.13 | 0.00 | 13.73 | 0.20 | 3.47 | 0.76 | 2.29 | 12.13 | 1.31 | 48.78 | 0.12 | 0.72 | 96.08 | 1037 | 1031 | 56 | 4.94 | 26.97 |
| SGM8 8/31/97 | 35 | 4.19 | 6.47 | 2.04 | 0.07 | 0.00 | 13.45 | 0.12 | 3.60 | 0.86 | 2.31 | 11.73 | 1.11 | 49.42 | 0.08 | 0.68 | 96.12 | 1031 | 1005 | 62 | 4.94 | 24.29 |
| SGM 9-7 2B-1 | Canister 9-7 | 3.88 | 10.85 | 1.67 | 0.15 | 0.28 | 13.44 | 2.54 | 3.04 | 1.31 | 2.09 | 12.19 | 1.32 | 47.67 | 0.55 | 0.06 | 101.03 | 1038 | 1026 | 44 | 4.39 | 31.57 |
| SGM 9-7 2T-2 | Canister 9-7 | 3.87 | 10.65 | 1.64 | 0.11 | 0.31 | 13.22 | 2.69 | 3.03 | 1.30 | 2.11 | 12.51 | 1.31 | 46.99 | 0.55 | 0.07 | 100.35 | 1038 | 1000 | 41 | 4.39 | 31.16 |
| SGM 9-7 3T-1 | Canister 9-7 | 3.81 | 10.59 | 1.63 | 0.11 | 0.28 | 13.12 | 2.67 | 2.99 | 1.28 | 2.05 | 12.08 | 1.32 | 46.79 | 0.55 | 0.06 | 99.34 | 1037 | 1011 | 44 | 4.39 | 31.51 |
| SGM 9-7 4B-1 | Canister 9-7 | 3.52 | 10.08 | 1.55 | 0.31 | 0.26 | 13.30 | 2.66 | 2.80 | 1.21 | 1.94 | 12.27 | 0.97 | 44.33 | 0.50 | 0.05 | 95.74 | 1052 | 1046 | 36 | 4.39 | 33.42 |
| SGM 9-7 4T-1 | Canister 9-7 | 3.46 | 10.02 | 1.62 | 0.26 | 0.25 | 13.00 | 2.87 | 2.78 | 1.21 | 1.94 | 12.01 | 1.03 | 44.43 | 0.50 | 0.05 | 95.43 | 1045 | 1035 | 39 | 4.39 | 33.72 |

| Glass ID | Ref | $Al_2O_3$ | $B_2O_3$ | CaO | $Cr_2O_3$ | CuO | $Fe_2O_3$ | $K_2O$ | $Li_2O$ | MgO | MnO | $Na_2O$ | NiO | $SiO_2$ | $TiO_2$ | $ZrO_2$ | Sum of Oxides | Old $T_L$ (°C) | New $T_L$ (°C) | Visc. (poise) | $Li_2O$ in frit | Waste Loading $Li_2O$ |
|---|---|---|---|---|---|---|---|---|---|---|---|---|---|---|---|---|---|---|---|---|---|---|
| SGM 9-7 4T-3 | Canister 9-7 | 3.42 | 10.05 | 1.46 | 0.25 | 0.26 | 12.84 | 2.90 | 2.76 | 1.21 | 2.20 | 12.42 | 0.99 | 44.28 | 0.50 | 0.08 | 95.61 | 1043 | 1011 | 37 | 4.39 | 34.35 |
| SGM 9-7 5B-1 | Canister 9-7 | 3.50 | 10.11 | 1.55 | 0.28 | 0.25 | 13.18 | 2.66 | 2.80 | 1.21 | 1.94 | 12.15 | 0.97 | 44.54 | 0.50 | 0.05 | 95.69 | 1048 | 1037 | 38 | 4.39 | 33.38 |
| LSFM-5 | 9 | 3.32 | 11.26 | 1.12 | 0.00 | 0.00 | 9.44 | 0.00 | 4.37 | 1.53 | 2.26 | 13.89 | 0.67 | 48.00 | 0.77 | 0.38 | 97.00 | 964 | 800 | 28 | 5.7 | 21.01 |
| LSFM-5 | 9 | 3.17 | 11.46 | 1.00 | 0.00 | 0.00 | 8.18 | 0.12 | 4.45 | 1.56 | 1.91 | 15.25 | 0.56 | 51.09 | 0.78 | 0.39 | 99.92 | 933 | 734 | 30 | 5.7 | 21.87 |
| LSFM-5 | 9 | 2.96 | 11.45 | 1.01 | 0.00 | 0.00 | 8.34 | 0.08 | 4.44 | 1.56 | 2.10 | 14.35 | 0.61 | 50.65 | 0.78 | 0.39 | 98.71 | 936 | 750 | 32 | 5.7 | 21.11 |
| LSFM-6 | 28 | 2.51 | 8.21 | 0.94 | 0.00 | 0.00 | 6.78 | 0.13 | 5.44 | 0.65 | 1.70 | 14.89 | 1.39 | 56.95 | 0.00 | 1.78 | 101.37 | 897 | 721 | 46 | 6.7 | 19.9 |
| LSFM-6 | 28 | 2.53 | 8.21 | 0.85 | 0.00 | 0.00 | 7.01 | 0.13 | 5.44 | 0.65 | 1.74 | 14.80 | 1.23 | 56.98 | 0.00 | 1.78 | 101.35 | 900 | 715 | 46 | 6.7 | 19.88 |
| LSFM-7 | 29 | 2.35 | 7.75 | 1.07 | 0.00 | 0.00 | 8.28 | 0.25 | 4.75 | 0.88 | 1.80 | 14.38 | 0.60 | 59.50 | 0.00 | 0.75 | 102.36 | 912 | 691 | 64 | 5.9 | 21.35 |
| LSFM-8 | 30 | 3.78 | 6.12 | 1.12 | 0.00 | 0.00 | 8.81 | 0.14 | 4.95 | 0.66 | 1.86 | 9.98 | 0.68 | 56.26 | 0.00 | 0.58 | 94.95 | 931 | 826 | 101 | 6.61 | 21.1 |
| LSFM-8 | 30 | 3.78 | 6.76 | 1.06 | 0.00 | 0.00 | 7.72 | 0.14 | 4.30 | 0.66 | 1.65 | 9.44 | 0.61 | 58.62 | 0.00 | 0.58 | 95.33 | 910 | 814 | 144 | 6.61 | 31.7 |
| LSFM-9 | 31 | 4.53 | 10.31 | 1.90 | 0.07 | 0.00 | 13.97 | 0.17 | 3.75 | 1.24 | 2.62 | 12.22 | 0.83 | 44.42 | 0.80 | 0.34 | 97.17 | 1073 | 993 | 28 | 5.7 | 32.29 |
| LSFM-9 | 31 | 4.65 | 7.35 | 1.29 | 0.10 | 0.00 | 12.74 | 0.20 | 5.12 | 0.70 | 2.76 | 10.62 | 0.99 | 53.94 | 0.05 | 0.63 | 101.14 | 1001 | 976 | 65 | 7 | 27.68 |
| LSFM-10 | 32 | 5.46 | 8.50 | 1.65 | 0.05 | 0.09 | 11.21 | 0.15 | 4.53 | 0.81 | 2.26 | 12.93 | 0.69 | 58.15 | 0.00 | 0.79 | 107.26 | 967 | 887 | 78 | 5.95 | 29.09 |
| SCM-2 (CELS analyzed) | 46 | 4.08 | 10.34 | 1.33 | 0.26 | 0.16 | 11.90 | 3.19 | 3.14 | 1.21 | 2.87 | 12.75 | 1.07 | 46.47 | 0.08 | 0.00 | 98.86 | 1018 | 990 | 41 | 4.62 | 31.18 |
| SCM (F21B) | 5 | 3.10 | 7.90 | 5.00 | 0.00 | 0.00 | 14.40 | 0.00 | 3.10 | 0.00 | 3.10 | 15.84 | 1.70 | 41.40 | 0.00 | 0.00 | 95.54 | 1090 | 894 | 14 | 4.6 | 29.46 |
| SCM-2 (F21 High Fe) | 60 | 1.64 | 7.50 | 4.99 | 0.00 | 0.00 | 18.06 | 0.00 | 3.00 | 0.00 | 0.99 | 13.87 | 3.08 | 39.38 | 7.50 | 0.00 | 100.01 | 1163 | 969 | 11 | 4 | 25.01 |
| SCM-2 (F21 Avg) | 60 | 7.43 | 7.50 | 4.62 | 0.00 | 0.00 | 12.53 | 0.00 | 3.00 | 0.00 | 2.74 | 13.87 | 1.44 | 39.38 | 7.50 | 0.00 | 100.00 | 1120 | 993 | 30 | 4 | 25 |
| SCM-2 (F21Composite) | 60 | 12.61 | 7.50 | 4.64 | 0.00 | 0.00 | 8.43 | 0.00 | 3.00 | 0.00 | 2.29 | 13.87 | 0.61 | 39.38 | 7.50 | 0.00 | 99.83 | 1084 | 938 | 69 | 4 | 24.87 |
| SCM-2 (F21 High Al) | 60 | 22.10 | 7.50 | 3.85 | 0.00 | 0.00 | 1.54 | 0.00 | 3.00 | 0.00 | 1.03 | 13.87 | 0.23 | 39.38 | 7.50 | 0.00 | 100.00 | 927 | 843 | 301 | 4 | 25 |

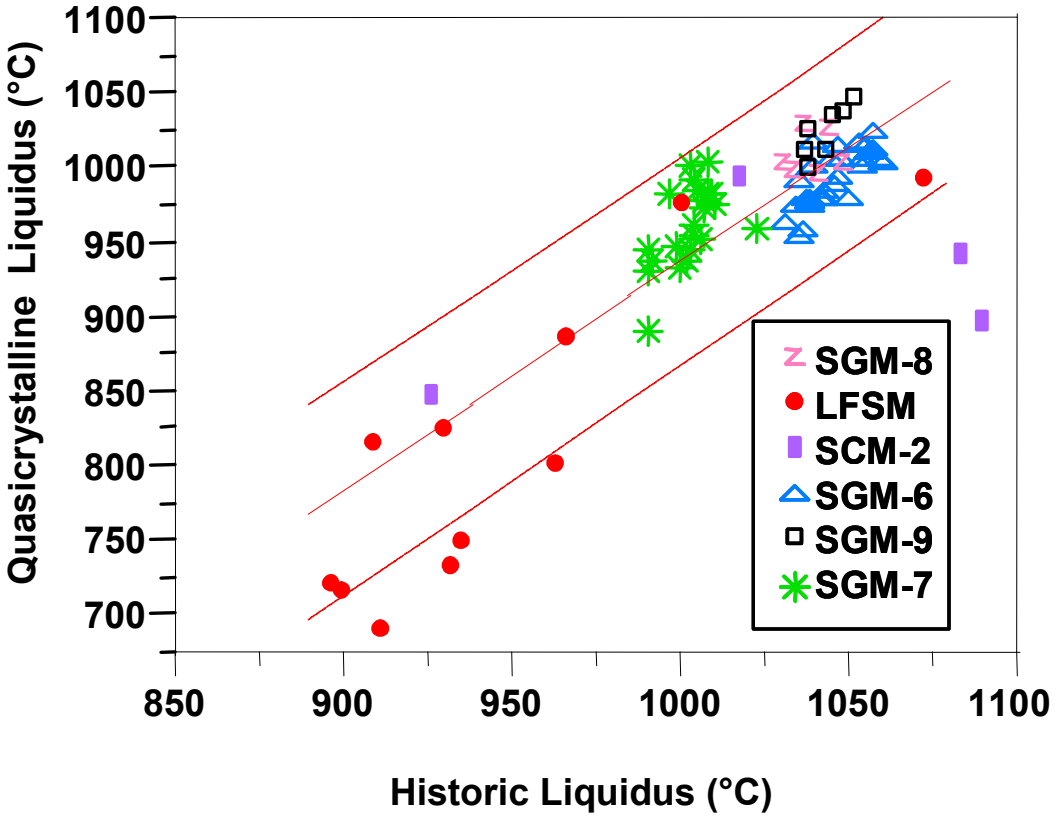


Figure 3. Comparison of the liquidus temperatures for various pilot scale melters calculated historically and with the newly implemented DWPF quasicrystalline model.

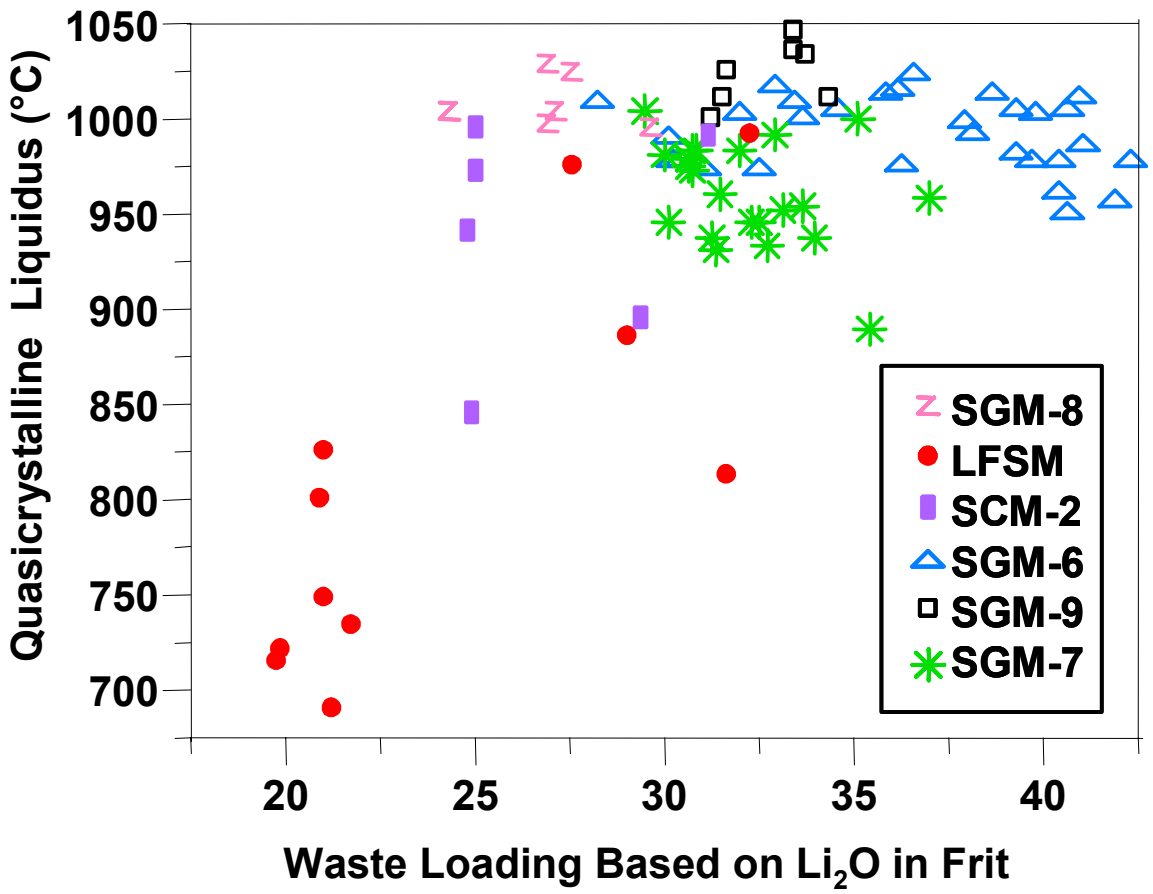


Figure 4. Comparison of the liquidus temperatures and waste loadings for various pilot scale melters calculated with the newly implemented DWPF quasicrystalline model.

# 3.0 SAMPLE ANALYSES

## 3.1 Visual Observation

The three samples were placed in the Savannah River Technology Center (SRTC) Shielded Cells, removed from their primary containers, and photographed, Figure 5. The pour stream sample (PC0033) had fallen out of its Pt boat in the DWPF melt cell and broken before it was shipped to SRTC. The pour stream sample had a varied appearance, most of it appeared black and shiny with a reflective surface but some of it appeared matte. The insert sample (PC0031) consisted of particles that were matte and dark gray to black with textured surfaces that had a gritty appearance. The upper pour spout bore sample (PC0006) appeared more uniform than the insert sample but not as reflective as the pour stream sample. The pour stream sample (PC033) was 29.169 grams, the upper pour spout bore sample (PC0006) was 45.181 grams, and the insert sample (PC0031) was 11.015 grams.

A

B

C

Figure 5. From top to bottom, A) black and shiny pour stream sample PC0033, B) dark gray and matte insert sample PC0031, and C) upper pour spout bore sample PC0006.

### 3.2 Elemental Analyses

Samples were prepared for chemical analyses by pulverizing a portion of each glass in a Wig-L-Bug using agate balls and vial. The pulverized sample was sieved using a 100-mesh (149 μm) brass sieve. The –100-mesh sample was used for the dissolutions. The glass samples were dissolved by two methods* to account for all of the elements of interest.

A standard reference glass, Approved Reference Glass #1 (ARG-1), was analyzed at the same time as the unknowns. Each standard and each unknown was dissolved in quadruplicate and one replicate analysis of each sample was performed. The quadruplicate analyses were averaged to create the data in Table IV. The Mixed Acid (MA) dissolutions were analyzed by Inductively Coupled Plasma – Emission Spectroscopy (ICP-ES) and ICP Mass Spectroscopy (ICP-MS). The Peroxide Fusion (PF) analyses were analyzed by both ICP-ES and ICP-MS as well. Samples which were dissolved by the MA dissolution were run at a 10X dilution and a 10 sigma confidence applied to the data. Samples which were dissolved by the PF were first run at a 10X dilution and then rerun at a 5X dilution and a 10 sigma confidence applied. The duplicate analyses were performed at the 5X dilution because of detection limit difficulties with B by ICP-ES. Samples which were analyzed by ICP-MS were run at a 10X dilution and a 6 sigma confidence applied.

When the data from the MA and PF analyses were compared to the ARG-1 standard glass analyses for each method, it was determined that the MA analyses were biased low for the ARG-1 standard for several key elements such as $SiO_2$. Moreover, the peroxide fusion method is more aggressive and ensured dissolution of the refractory spinels and $Cr_2O_3$ in the insert and upper pour spout bore samples. Comparisons of the MA and PF analyses to the known composition of the ARG-1 glass standard were used to determine which set of values to use for which elements as indicated in Table IV. For example, the MgO analyses from the peroxide fusion appeared biased high for the ARG-1 standard [47] while the mixed acid MgO analyses appeared to be at the value reported for the ARG-1 standard. However, the MgO values reported in Table IV are those determined from the peroxide fusion dissolution because the mixed acid dissolution left visible undissolved solids in all four quadruplicate PC0031 dissolutions. Likewise, the mixed acid and peroxide fusion analyses were the same and on target for $Cr_2O_3$ as reported in ARG-1 glass [47]. However, the peroxide fusion analyses are reported in Table IV preferentially because of the undissolved solids found in the mixed acid digestions for PC0031. Due to the difficulty with dissolution of PC0031 when the mixed acid dissolution was used, the peroxide fusion data are reported in Table IV except for $Na_2O$ and $ZrO_2$ because these elements cannot be achieved in a sodium peroxide fusion performed in a zirconium crucible.

In order to provide a representation of the expected composition of the pour stream sample, the analysis of SME batch 245 and MFT batch 245 were converted to oxides using the DWPF Product Composition Control System (PCCS) spreadsheet. Table IV gives the composition of

* ADS-2502 – Sodium Peroxide/Sodium Hydroxide Dissolutions of Sludge and Glass for Elemental and Ion Analysis.
ADS-2227 – Acid Dissolution of Glass and Sludge for Elemental Analysis.

the three DWPF samples as well as the composition of the SRTC Tank 40 qualification glass sample and the measured composition of SME Batch 245 [48] and MFT batch 245 [49].

The composition of the pour stream sample resembles the SRTC Tank 40 qualification glass made with Frit 320 in the Shielded Cells Facility in $Al_2O_3$, MgO, $B_2O_3$, CaO, CuO, $Li_2O$, MgO, MnO, $P_2O_5$, and $U_3O_8$ (Table IV) as it should if the Tank 40 sample was representative. The pour stream sample resembles most of the major components as determined by analysis of SME batch 245 (Table IV). This is verified in Table V as the ratios of most components in SME batch 245 divided by the concentrations in the pour stream sample (PC0033) are close to 1.0 as they should be. The SME batch 245 analyses appear to be biased high or the pour stream samples biased low for $Al_2O_3$, $B_2O_3$, CaO, $Fe_2O_3$, NiO and $U_3O_8$ by 15-20%. The MFT batch 245 analyses divided by the concentrations in the pour stream sample (PC0033) are ~1.0 except for the $Al_2O_3$ and $B_2O_3$ analyses which are biased by ~20% (Table IV).

The compositions of the analyses reported in Table IV were used to calculate a predicted glass viscosity, liquidus temperature and waste loading. The six MFT analyses provided in Reference 49 were entered into the DWPF PCCS SME spreadsheet to calculate the MFT predicted glass properties in exactly the same manner as the SME predicted glass properties. The predicted viscosity based on the vitrified SME 245 product was ~36 poise, the predicted viscosity based on the vitrified MFT product was 43.48 poise. The predicted viscosity based on the pour stream sample analysis was 46.05 poise in agreement with vitrified MFT product analyses to within 2.5 poise. The predicted liquidus based on the vitrified SME 245 product was 1038°C, the predicted liquidus based on the vitrified MFT 245 product was 987°C. The predicted liquidus based on the pour stream sample analysis is 997°C in agreement with the MFT analyses to within 10°C. The waste loadings predicted from the SME, MFT and pour spout analyses are 39.32, 34.74, and 38.53, respectively, based on the reported $Li_2O$ content [45]. The SME waste loading and the pour spout sample waste loading agree to within 0.8 wt% while the MFT waste loading and the pour spout sample agree to within 3.79 wt%.

The composition of the upper pour spout bore sample (PC0006) was very different from the pour stream sample (PC0033) and very different from the MFT and SME analyses. The pour spout bore sample was deficient in $Al_2O_3$, $B_2O_3$, CaO, $Li_2O$, $Na_2O$, $U_3O_8$ and $SiO_2$ (see Table V). Based on the relative $Li_2O$ content of the pour stream sample (PC0033) relative to the bore sample (PC0006) it is estimated that the upper pour spout bore sample was ~62 wt% glass (Table VI). Based on the relative $SiO_2$ content of these samples it is estimated that the upper pour spout bore sample is ~52 wt% glass (Table VI). The upper pour spout bore sample was enriched in $Cr_2O_3$ over the pour stream sample by 35.9X, enriched in $Fe_2O_3$ by only 2.6X, and enriched in NiO by 15.4X compared to the pour stream. Based on the analyzed compositions given in Table IV and the X-ray diffraction spectra for this sample discussed in a Section 2.7 of this report, the number of moles of NiO, $Cr_2O_3$, and $Fe_2O_3$ over those reported in the pour stream were calculated. Based on these molar compositions it could be determined that 0.11 moles of $NiFe_2O_4$ and 0.034 moles of $NiCr_2O_4$ spinels comprised the remainder of the bore samples. When converted to weight percent, a mass balance indicated that the deposits were ~62 wt% glass, 25.78 wt% $NiFe_2O_4$ (trevorite) and 7.7 wt% $NiCr_2O_4$ (Table VI). The upper pour spout bore is also highly enriched in noble metal components; especially $Rh_2O_3$ and $RuO_2$ (see Table VII).

The insert sample PC0031 was enriched the most in $Cr_2O_3$ over both the pour stream sample (PC0033) and upper pour spout bore sample (PC0006). The insert sample contains less $Fe_2O_3$ and NiO than the upper pour spout bore. This indicates that less $NiFe_2O_4$ spinels are accumulating in this area, e.g. the mass balance analyses indicate ~16.4 wt% $NiFe_2O_4$ (see Table VI). However, the high $Cr_2O_3$ content supported by the XRD identification of a $Cr_2O_3$ only phase indicates that there may be a reaction occurring with the hot glass and the Cr in the Inconel® 690 alloy that the insert is made of, e.g. an oxidized film of $Cr_2O_3$ may be forming to which some molten glass adheres. Since the sample received had "spalled off" the insert as it cooled it is likely that the sample contained a good deal of the oxidized $Cr_2O_3$ film from the Inconel® 690. The mass balance indicates that ~21 wt% $Cr_2O_3$ comprises the deposits analyzed. Table V presents the ratios of the major components of the pour stream sample to the other compositions from Table IV. The insert sample is also enriched in noble metals (Table VII).

Table IV. Measured Compositions of the DWPF Melter #2 Samples Compared to SRTC Tank 40 Glass and DWPF SME Batch 245 and MFT Batch 245 (in Oxide Wt.%)

| Oxide | Dissolution/ Analysis Methods | Pour Stream (PC0033) | Upper Pour Spout Bore (PC0006) | Insert (PC0031) | SRTC TK 40 Glass[50] | SME Batch 245[48] | MFT Batch 245[49] |
|---|---|---|---|---|---|---|---|
| **$Ag_2O$** | **PF/ICPMS** | 0.0072 | BDL | 0.006 | NM | NM | NM |
| **$Al_2O_3$** | **PF/ICPES** | 4.33 | 2.40 | 2.54 | 4.93 | 5.59 | 5.04 |
| **$B_2O_3$** | **PF/ICPES** | 4.33 | <2.93 | <2.68 | 4.87 | 5.21 | 5.26 |
| **BaO** | **PF/ICPES** | 0.03 | 0.02 | 0.01 | NM | NM | NM |
| **CaO** | **PF/ICPES** | 1.48 | 0.95 | 0.87 | 1.53 | 1.69 | 1.26 |
| **CdO** | **PF/ICPES** | 0.05 | 0.05 | 0.05 | NM | NM | NM |
| **$Cr_2O_3$** | **PF/ICPES** | 0.15 | 5.38 | 21.22 | 0.31[a] | 0.12 | 0.11 |
| **CuO** | **PF/ICPES** | 0.09 | 0.07 | 0.03 | 0.14 | 0.03 | 0.03 |
| **$Fe_2O_3$** | **PF/ICPES** | 13.64 | 36.03 | 25.19 | 16.16 | 15.69 | 14.07 |
| **$K_2O$** | **PF/ICPES** | BDL | BDL | BDL | NM | 0.1381 | 0.10 |
| **$La_2O_3$** | **PF/ICPES** | 0.04 | 0.04 | 0.05 | NM | NM | NM |
| **$Li_2O$** | **PF/ICPES** | 4.75 | 2.93 | 3.48 | 5.30 | 4.85 | 5.16 |
| **MgO** | **PF[d]/ICPES** | 1.28 | 1.22 | 1.48 | 1.30 | 1.31 | 1.10 |
| **MnO** | **PF/ICPES** | 1.67 | 2.35 | 3.29 | 1.84 | 1.73 | 1.54 |
| **$Na_2O$** | **MA/ICPES** | 11.01 | 6.30 | 6.26 | 12.61 | 11.39 | 11.02 |
| **NiO** | **PF/ICPES** | 0.60 | 9.25 | 5.84 | 0.74 | 0.71 | 0.63 |
| **$P_2O_5$** | **PF/ICPES** | 0.60 | <0.63 | <0.63 | 0.74 | <0.22 | NM |
| **$SO_4$** | **PF/ICPES** | c | c | c | NM | <0.25 | <0.27 |
| **$SiO_2$** | **PF/ICPES** | 46.87 | 24.26 | 24.55 | 51.2 | 45.67 | 48.11 |
| **$SnO_2$** | **PF/ICPES** | 0.21 | 0.20 | 0.19 | NM | NM | NM |
| **SrO** | **PF/ICPES** | 0.30 | 0.20 | 0.20 | NM | NM | NM |
| **$Rh_2O_3$** | **PF/ICPMS** | 0.0033 | 0.271 | 0.058 | NM | NM | NM |
| **$RuO_2$** | **PF/ICPMS** | 0.030 | 1.712 | 0.296 | NM | NM | NM |
| **$TiO_2$** | **PF/ICPES** | 0.04 | 0.03 | 0.11 | NM | 0.05 | 0.05 |
| **$U_3O_8$** | **PF/ICPES** | 3.45 | 2.63 | 2.45 | 4.06 | 4.22 | 3.80 |
| **ZnO** | **MA/ICPES** | 0.09 | 0.16 | 0.17 | NM | NM | NM |
| **$ZrO_2$** | **MA/ICPES** | 0.07 | 0.03 | 0.03 | NM | BDL | 0.09 |
| **SUM (w/o <)** | | 95.12 | 96.48 | 98.37 | 105.86 | 98.4 | 97.37 |
| **Calculated Viscosity @1150°C (poise)** | | 46.05 | N/A | N/A | 38.99 | 35.91 | 43.48 |
| **Calculated Liquidus (°C)** | | 997 | N/A | N/A | 1056 | 1038 | 987 |
| **Calculated WL ($Li_2O$)** | | 38.53[b] | N/A | N/A | 36.10 | 39.32[b] | 34.74[b] |

(NM-Not Measured; BDL-Below Detection Limit; N/A-Not Applicable; MA-Mixed Acid dissolution; PF- Peroxide Fusion dissolution; WL-Waste Loading)

[a] Sample prepared in stainless steel grinder for Sludge Batch 2 (SB-2) qualification with Frit 320.

[b] Calculated using a value for $Li_2O$ in the normalized frit of 8.13 wt% based on a weighted average of Frit 320 Lots 5, 8, and 13 in the ratio of 1:1:2.

[c] $SO_4$ analyses were indeterminate as the ARG-1 standards were reported to contain ~1.2 wt% $SO_4$. The SRTC Mobile Laboratory performed an analysis of the ARG-1 glass in duplicate using a $LiBO_2$ dissolution and a different ICP-ES. In addition, a sodium peroxide fusion was performed with a water uptake and an additional analysis for $SO_4$ performed by Ion-Chromotography (IC). The results indicated <0.3 wt% and <0.08 wt% $SO_4$ in the ARG-1 glass, respectively. In addition, <0.25 $SO_4$ was reported in the SME-245 analyses and only 0.36 wt% $SO_4$ was reported in SB2 before frit dilution [51]. Subsequent$SO_4$ analyses demonstrated that these $SO_4$ analytic results represented the detection limit for SO4 for the methods being used at the time this analysis was performed.

d Peroxide fusion was used for Mg analysis instead of mixed acid (usual method for this element) since undissolved solids had been found in the mixed acid digestion of sample PC0031.

Table V. Ratio of Major Components of the Pour Stream Sample to the Upper Pour Stream Bore Sample, to the Insert Sample, and to the SME 245 and MFT 245 Analyses.

| | Insert /Pour Stream | Upper Pour Spout Bore /Pour Stream | SME batch 245/ Pour Stream | MFT batch 245/ Pour Stream |
|---|---|---|---|---|
| **$Al_2O_3$** | 0.59 | 0.55 | 1.29 | 1.16 |
| **$B_2O_3$** | N/A | N/A | 1.20 | 1.21 |
| **CaO** | 0.59 | 0.64 | 1.14 | 0.85 |
| **$Cr_2O_3$** | 141.47 | 35.87 | 0.8 | 0.73 |
| **$Fe_2O_3$** | 1.85 | 2.64 | 1.15 | 1.03 |
| **$Li_2O$** | 0.73 | 0.62 | 1.02 | 1.09 |
| **MgO** | 1.16 | 0.95 | 1.02 | 0.86 |
| **MnO[b]** | 1.97 | 1.41 | 1.04 | 0.92 |
| **$Na_2O$** | 0.56 | 0.57 | 1.03 | 1.01 |
| **NiO** | 9.73 | 15.42 | 1.18 | 1.05 |
| **$SiO_2$** | 0.52 | 0.52 | 0.97 | 1.03 |
| **$U_3O_8$** | 0.71 | 0.76 | 1.22 | 1.10 |

[b]ADS method parameter for Mn > ±10% for pour stream and insert samples.

Table VI. Mass Balance for Samples Based on Data in Table IV.

| | Pour Stream (PC0033) Frit 320 | Upper Pour Spout Bore (PC0006) Frit 320 | Insert (PC0031) Frit 320 |
|---|---|---|---|
| **Calculated Glass (wt%) Based on $Li_2O$ (or $SiO_2$) in Pour Stream** | 100 | 62 (51.8) | 73 (52.4) |
| **Calculated $NiFe_2O_4$ Spinel (wt%)** | 0 | 25.78 | 16.4 |
| **Calculated $NiCr_2O_4$ (wt%)** | 0 | 7.70 | 0 |
| **Calculated $Cr_2O_3$ (wt%)** | 0 | 0 | 21.07 |
| **$RuO_2 + Rh_2O_3$** | 0.03 | 1.98 | 0.36 |
| **SUM** | 100.03 | 97.46 (87.26) | 110.83 (90.23) |

### 3.3 Noble Metal Analyses

The solutions that resulted from both the acid dissolution and the peroxide fusion of the three samples were analyzed by Inductively Coupled Mass Spectroscopy (ICP-MS) for noble metals to gain more detailed information about the composition of the samples. Concentrations in weight percent along with the respective concentrations measured in the SRTC Tank 40 qualification sample are given in Table VII. The data from the SB2 pour stream and insert are also given in Table VII for comparison. The concentrations not in parentheses are those determined by the peroxide fusion (PF) followed by ICP-MS analysis. A peroxide fusion was used to ensure that all the refractory spinels in the pour spout and insert samples were dissolved because the noble

metal, Ru as $RuO_2$, is most often in the center of an insoluble spinel crystal where it has acted as a nucleating site. The concentrations in Table VII that are in parentheses are those measured by ICP-MS on the mixed acid (MA) dissolutions which are not as aggressive as the peroxide fusion dissolution. Therefore, the PF data is used preferentially in this report.

Table VII. Comparison of the Noble Metals (wt.%) of the SRTC Tank 40, Pour Stream, Upper Pour Spout Bore, and Insert Glasses.

| Isotope | SB2 Pour Stream Glass (August 2002) | SB2 Insert Glass (August 2002) | SB2 Pour Stream Glass (PC0033) | SB2 Upper Pour Spout Bore (PC0006) | SB2 Insert (PC0031) | Ratio Insert/ Pour Stream[b] | Ratio Upper Spout Bore/ Pour Stream |
|---|---|---|---|---|---|---|---|
| Ru (PF)<br>Ru (MA) | NA<br>(7.8E-03) | NA<br>(5.05E-07) | 0.023<br>(6E-03) | 1.3<br>(0.37) | 0.23<br>(0.058) | 10<br>(9.67) | 56.52<br>(61.67) |
| Rh (PF)<br>Rh (MA) | NA<br>(6.2E-04) | NA<br>(9.68E-05) | 0.0027<br>(NA) | 0.22<br>(0.053) | 0.047<br>(0.013) | 17.41<br>(NA) | 81.48<br>(NA) |
| Pd (PF)<br>Pd (MA) | NA<br>(3.4E-04) | NA<br>(7.02E-02) | NA<br>(NA) | NA<br>(5.5E-04) | NA<br>(NA) | NA<br>(NA) | NA<br>(NA) |
| Ag (PF)<br>Ag (MA) | NA<br>(4.2E-03) | NA<br>(6.69E-02) | 0.0067<br>(7.3E-03) | NA<br>(0.012) | 0.006<br>(0.004) | (NA)<br>0.55 | NA<br>(1.64) |

[b] This ratio should be ~0.47 because of dilution of the glass components by material from the insert (see text).

Based on the peroxide fusion (PF) data in Table VII, the noble metals, Ru and Rh were 56 to 81 times more concentrated in the upper pour spout bore than in the pour stream. The Ru and Rh were 10 and >17 times more concentrated in the insert glass. The mixed acid (MA) concentrations give similar results for the ratios for Ru accumulations in the upper pour spout bore and insert. While the absolute magnitude of the individual concentrations from the mixed acid dissolution is less, the ratios of the noble metals accumulations are similar based on the two dissolutions.

### 3.4 REDOX Analyses

To prepare samples for REDOX analysis, portions of the pour stream sample (PC0033) were pulverized using the Wig-L-Bug in the SRTC Shielded Cells. Oxidation concerns of finely ground material precluded the use of material previously pulverized for compositional analysis. The Environmental Assessment (EA) glass was prepared by grinding it in a Tekmar grinder outside the SRTC Shielded Cells as a control. EA glass is reported to have a REDOX ($Fe^{2+}/Fe^{tot}$) of ~ 0.18 [52]. Dissolutions of triplicate samples were performed using –100 mesh material prepared in the same manner as the material for compositional analysis. The dissolution of the samples was conducted using the procedure from the SRTC Mobile Laboratory [53]. The dissolution and dilution portions of the procedure were performed in the SRTC Shielded Cells. The spectrophotometric analysis were performed in a radiohood.

Table VIII gives the results of the triplicate REDOX analyses of PC0033 and the EA glass standard. The measured REDOX of the EA glass was greater than expected. A portion of the EA glass that had been ground and transferred to the SRTC Shielded Cells still remained in a non-radioactive laboratory in SRTC (B-118). This sample was placed under a high powered optical microscope and it was discovered that it was contaminated with metal filings from the Tekmar grinder used to grind it. This should not affect the REDOX of the PC0033 sample since it was ground with a Wig-L-Bug that does not contain metal parts. Therefore, no bias correction was made to the REDOX of the PC0033 sample, which was 0.20. The REDOX of the pour stream sample taken in August 2002 was 0.21 [54].

A second EA glass standard was ground with the Wig-L-Bug to prevent metal contamination and the REDOX of PC0033 and the EA glass standard re-measured in triplicate in the SRTC Shielded Cells (see Table VIII). This set of analyses gave a blank corrected EA glass standard value of $Fe^{+2}/\Sigma Fe$=0.24 versus the reported standard value of 0.18 indicating that the problems with iron contamination had been avoided by using the Wig-L-Bug. The remeasured values for the triplicate PC0033 samples when averaged were 0.20 in agreement with the previous values determined in Table VIII.

The predicted REDOX of SME batch 245 was 0.17 based on the {[F]-[3N]} REDOX correlation [55] and 0.15 based on the new Electron Equivalents REDOX correlation [56] and the predicted REDOX of SME batch 224 (corresponding to the August pour stream sample from SB2) had a predicted redox 0.19 based on the {[F]-[3N]} REDOX correlation [48]. This indicates that the REDOX model [56], predictions, and batching in the DWPF SRAT and melter are working correctly and are on target.

At a REDOX $Fe^{+2}/\Sigma Fe$=0.20 the oxygen fugacity of the DWPF melt pool is $\log f_{O_2} = -5.5$ which means that 30% of the uranium is there as $U^{+5}$, ~15% is present as $U^{+4}$ and the remainder (~55%) is present as $U^{+6}$ from the known Electromotive Force (EMF) series developed by Schreiber for DWPF glass [57]. The oxygen fugacity will later (Section 4.2) be related to the corrosivity of the Inconel® 690.

### 3.5 Glass Density Measurement

The density of the pour stream sample (PC0033) was measured by water displacement. The density of the NIST standard material SRM 1826b is 2.549 g/cc. It was measured in the shielded cells as 2.503 g/cc. The density measured on sample PC0033, the pour stream glass, was 2.662 g/cc. If the density of the pour stream glass is bias corrected to the NIST standard value then the density of the pour stream glass is 2.708 g/cc.

Table VIII. REDOX of Pour Stream (PC0033) Glass Prepared in the SRTC Shielded Cells.

| | | Absorbance | | | |
|---|---|---|---|---|---|
| **Set** | **Sample** | **$Fe^{2+}$** | **$Fe^{tot}$** | **Blank Corrected $Fe^{2+}/Fe^{tot}$** | **Blank Corrected Average ($Fe^{2+}/Fe^{tot}$)** |
| 1 | Blank | 0.0000 | 0.0000 | | |
| 1 | EA-1 | 0.1325 | 0.3657 | 0.3623 | |
| 1 | EA-2 | 0.1567 | 0.3628 | 0.4319 | |
| 1 | EA-3 | 0.1417 | 0.3323 | 0.4264 | 0.41 |
| 1 | PC0033-1 | 0.0745 | 0.3374 | 0.2208 | |
| 1 | PC0033-2 | 0.1307 | 0.6690 | 0.1953 | |
| 1 | PC0033-3 | 0.0630 | 0.3487 | 0.1807 | 0.20 |
| 2 | Blank | 0.008 | 0.025 | | |
| 2 | EA-1 | 0.094 | 0.388 | 0.2369 | |
| 2 | EA-2 | 0.086 | 0.382 | 0.2185 | |
| 2 | EA-3 | 0.087 | 0.342 | 0.2492 | 0.23 |
| 2 | PC0033-1 | 0.086 | 0.394 | 0.2114 | |
| 2 | PC0033-2 | 0.088 | 0.427 | 0.1990 | |
| 2 | PC0033-3 | 0.075 | 0.377 | 0.1903 | 0.20 |

### 3.6 Contained Scanning Electron Microscopy (CSEM)

The <200 mesh crushed samples from the dissolutions were used for contained scanning electron microscopy with energy dispersive spectroscopy (CSEM/EDS) rather than small chunks of samples as used in the previous study [54]. During visual and x-ray diffraction analysis the pour stream sample appeared homogeneous, therefore only one pour stream sample was prepared. One insert and one upper bore sample were also prepared. The CSEM analysis of the pour stream sample revealed uniformity across the entire sample. Examination of several fragments of the pour stream glass (PC0033) was unremarkable and showed no crystallization. The EDS spectrums of various pour stream samples were typical of a homogeneous DWPF-type glass.

The insert sample viewed at 500x appeared to have more surface texture than a typical glass sample. A single grain is shown in Figure 6 that has a coating of a high atomic weight element on the left side (see lighter shaded region on left side of left grain). The corresponding EDS spectra of the left hand side of the grain shown in Figure 7 which indicates that it is rich in Fe and Cr compared to the right hand side of the same grain which has an EDS spectra typical of glass (Figure 8). The coating appears to be a portion of the Inconel® 690 to which the once molten glass had adhered.

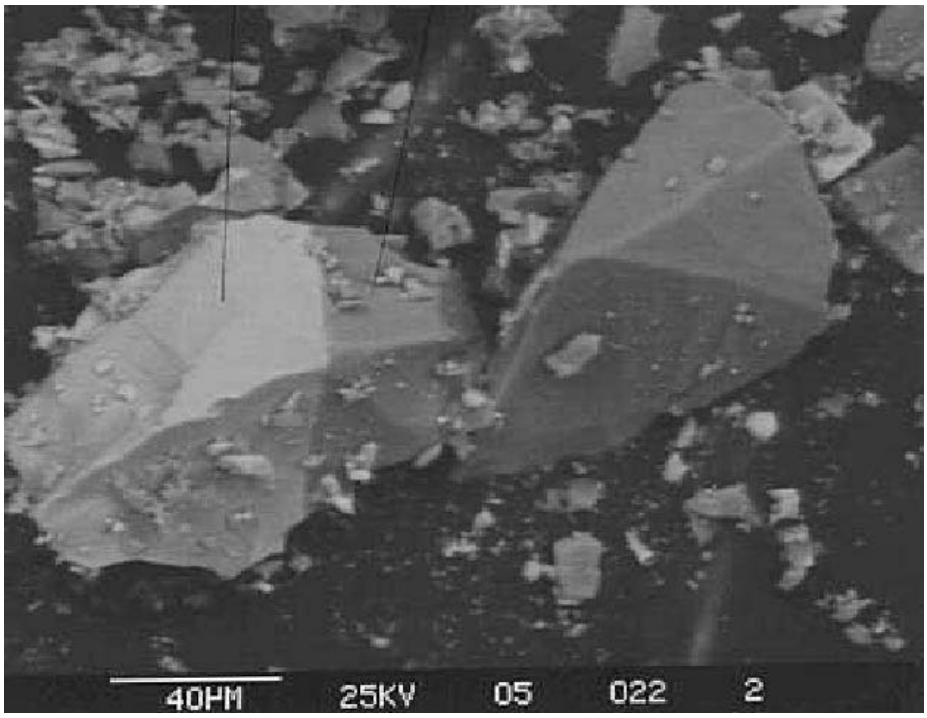


Figure 6 .Representative micrograph of the insert sample glass (PC0031), 500X in back scatter which makes high atomic element cations appear "lighter" than the remaining matrix.

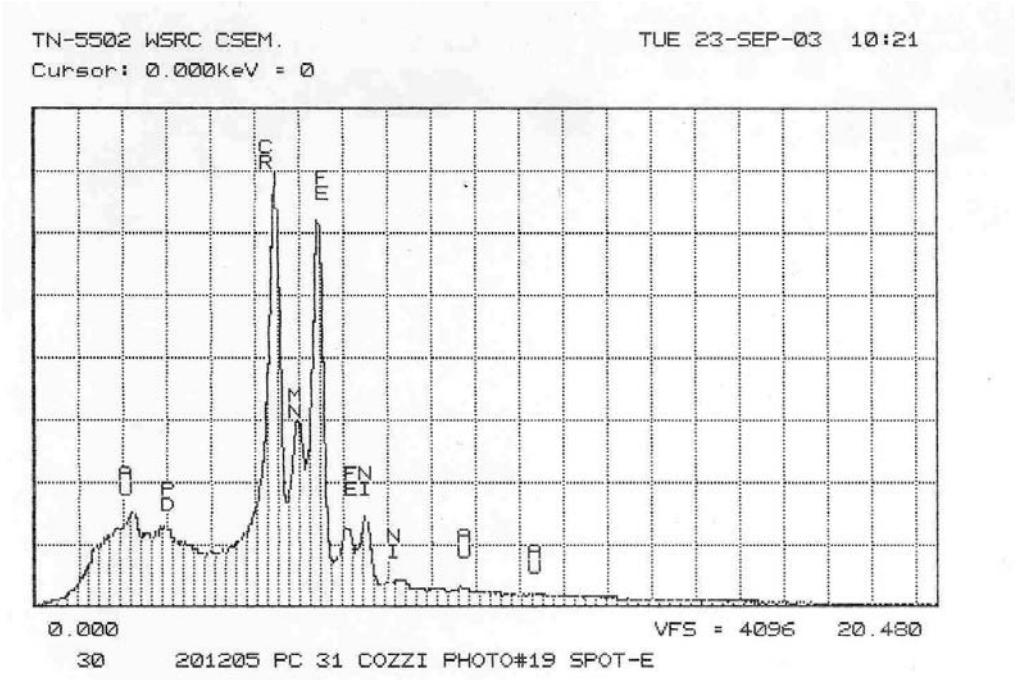


Figure 7. EDS spectrum of the bright coating (left hand side of sample) on the insert sample glass (PC0031). Sample is coated with Au and Pd to minimize charging.

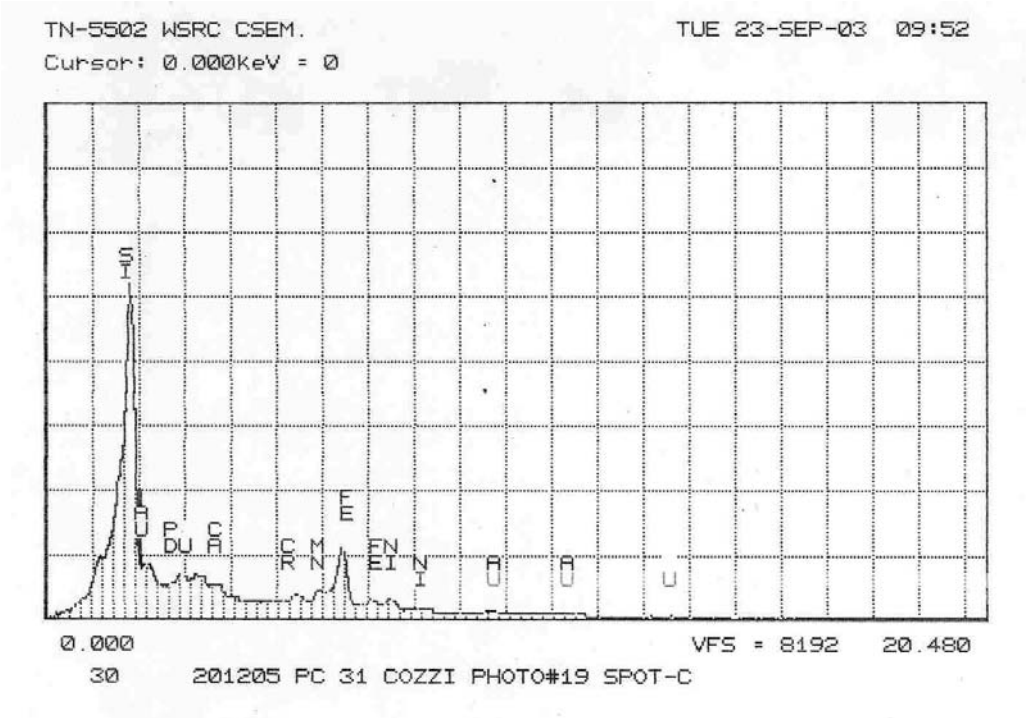


Figure 8. EDS spectrum of the right hand side of the grain of the insert sample glass (PC0031) exhibiting the coating in Figure 6. Sample is coated with Au and Pd to minimize charging. EDS spectra is typical of glass.

The CSEM/EDS of the insert sample revealed copious amounts of spinels as shown in the EDS spectra shown in Figure 9. Some of the spinels are more enriched in Cr than others (compare Figure 9 top and bottom). The non-crystalline portion of the sample gave a spectra typical of glass and demonstrated that the U component is in the glassy phase (Figure 10). The EDS spectra did not indicate that the spinels were associated with $RuO_2$. The sodium chromium sulfate observed in previous pour spout sampling [20, 22, 54] was not observed in any of the samples analyzed in this study and that is consistent with the lack of detectable S in the samples during chemical analysis (see Table IV).

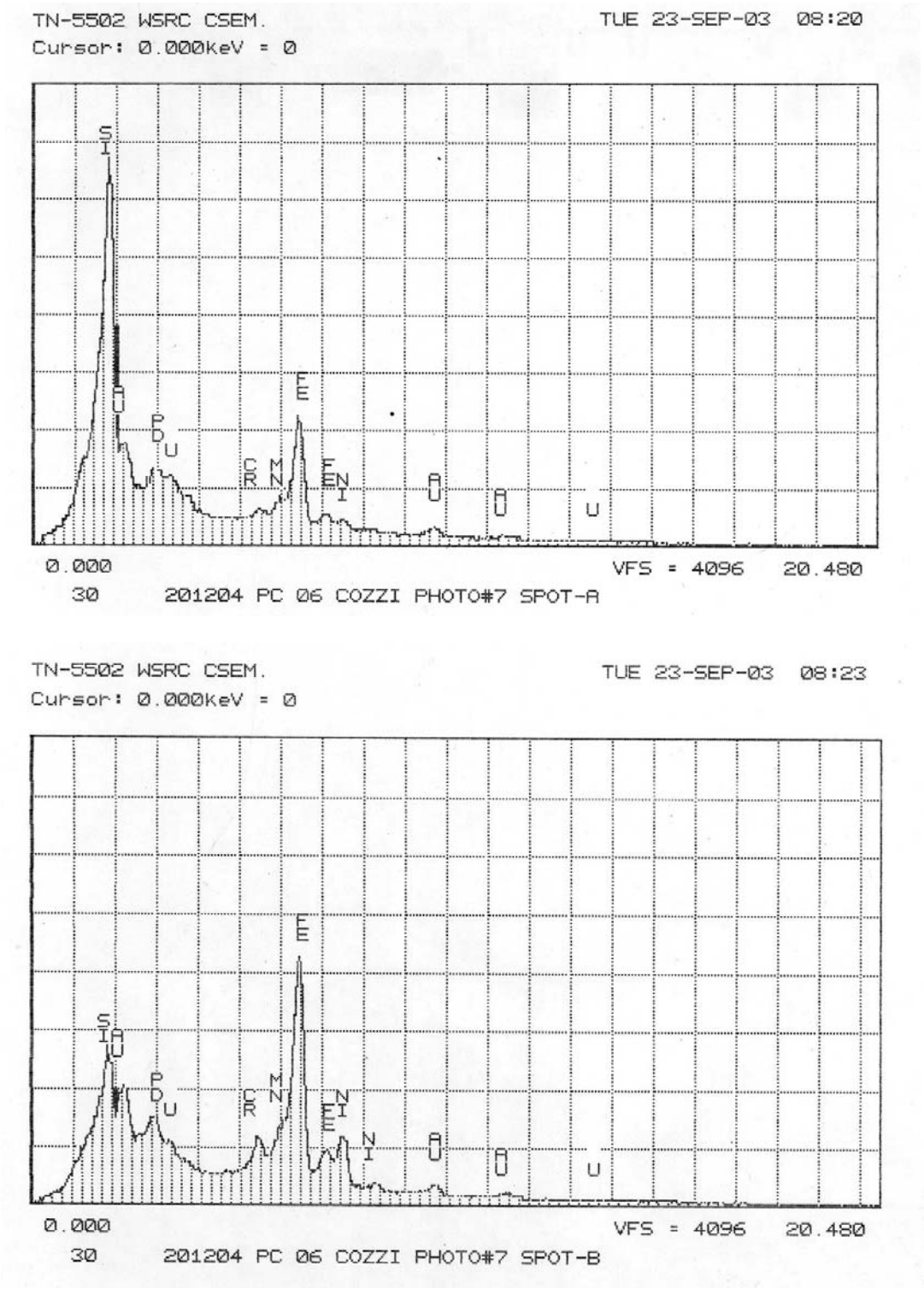


Figure 9. EDS spectra of chromium and iron rich spinels in insert sample glass (PC0006).

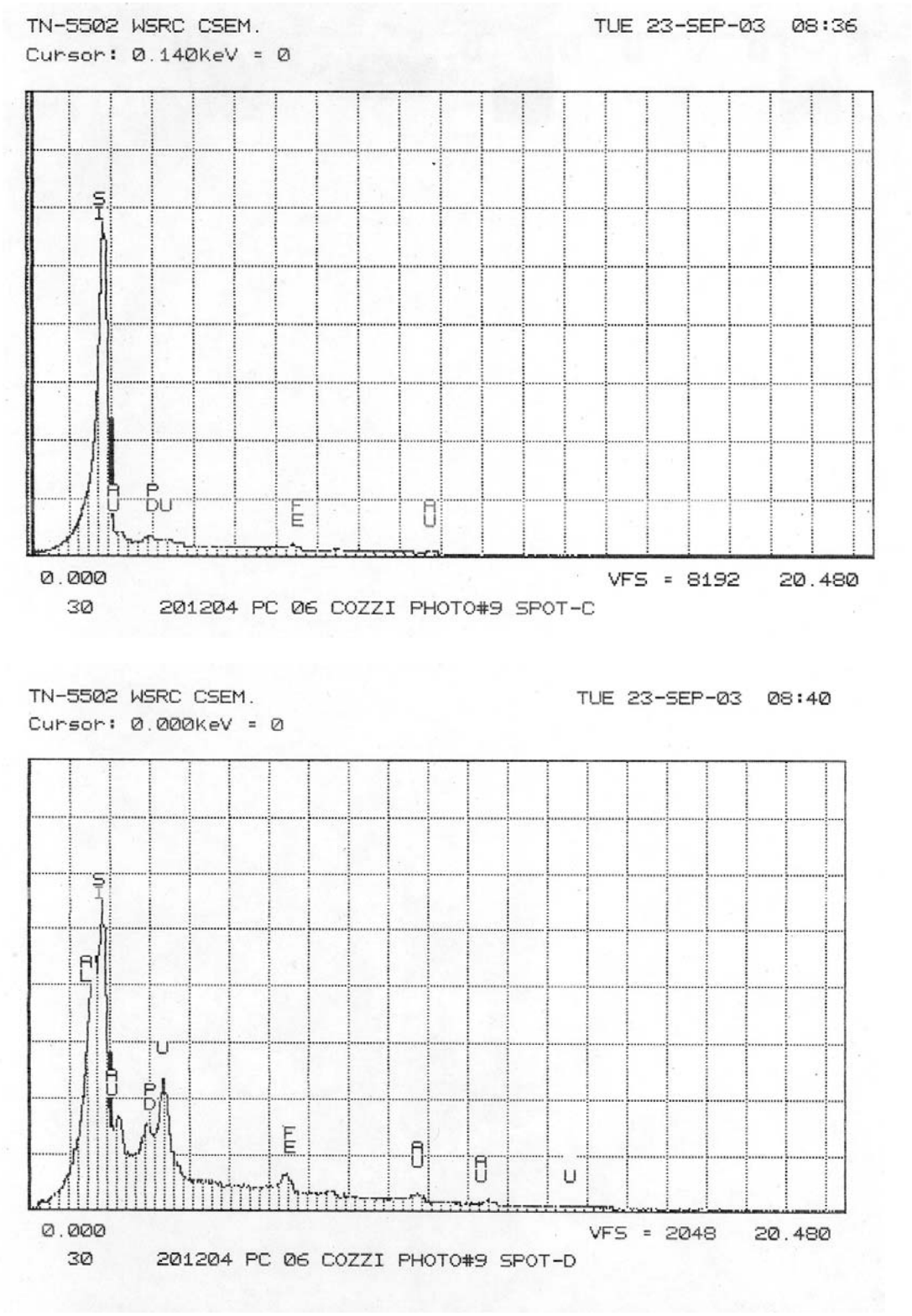


Figure 10. EDS spectra from the insert sample (PC0006) showing the composition of typical glass including the uranium component.

### 3.7 Contained X-ray Diffraction Analysis (CXRD)

For contained x-ray diffraction analysis (CXRD), the samples from the pour stream, upper pour stream bore, and insert samples were limited in size to reduce personnel dose. As with the CSEM samples, the small size of the CXRD samples limit the representative nature of the samples. For that reason three different portions of the pour stream were analyzed. Although large samples are preferred for improved signal to noise ratios, the ALARA program encourages the minimization of personnel exposure to radioactive samples.

The XRD pattern of two of the three pour stream samples was typical of a borosilicate glass and free of any indicators of crystalline matter (see Figure 11) except for potential stainless steel (ss) contamination from grinding. A third sample had been dropped on the deck of the DWPF melt cell where a saw with an alumina blade had recently been used to cut the core samples from Melter #1. The CXRD spectra of this sample indicated the presence of corundum ($Al_2O_3$) and possibly $NaAl_{11}O_{17}$ contamination.

The XRD analysis of the insert sample indicated the presence of glass, spinel, and chrome oxide (Figure 12). Along with the amorphous hump associated with a glassy phase, a spinel phase and a chromium oxide phase (eskolaite[†]) were identified. The spinel phase most likely resembles trevorite[‡] with chromium partially substituting for iron and iron partially substituting for nickel, based on the EDS spectrum shown in Figure 9. With 0.15 wt % $Cr_2O_3$ in the pour stream (Table IV) and ~141X enrichment in $Cr_2O_3$ in the insert sample (Table V), corrosion (oxidation) of the Inconel® 690 insert in the air rich environment of the insert is most likely the primary source. Therefore, the molten glass and the Inconel® 690 insert are chemically interacting in this hot oxidizing environment.

[†] Eskolaite. International Centre for Diffraction Data (ICDD) card 74-0326 $Cr_2O_3$
[ƒ] Ken Imrich personnel communication October 20, 2003
[‡] Trevorite ICDD card 86-2267 $NiFe_2O_4$

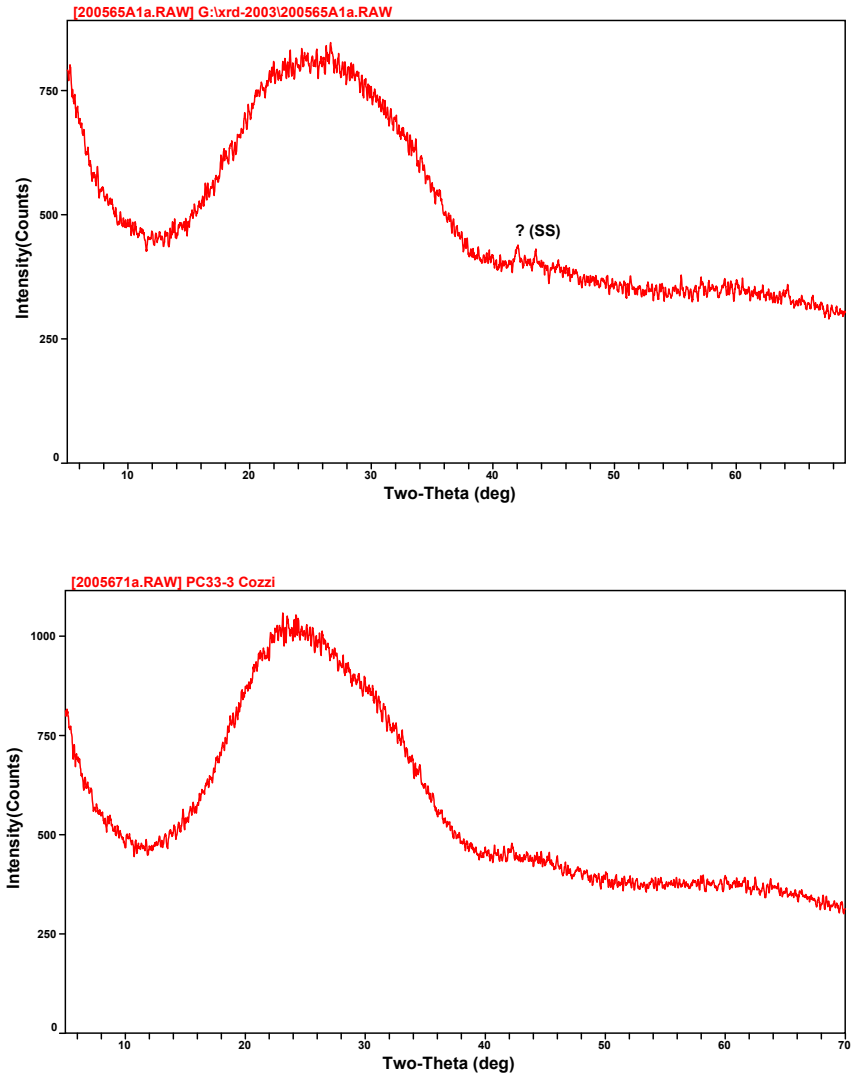


Figure 11. CXRD spectra of two of the three pour stream samples analyzed (PC0033) showing that the pour stream does not contain any spinels or other crystals.

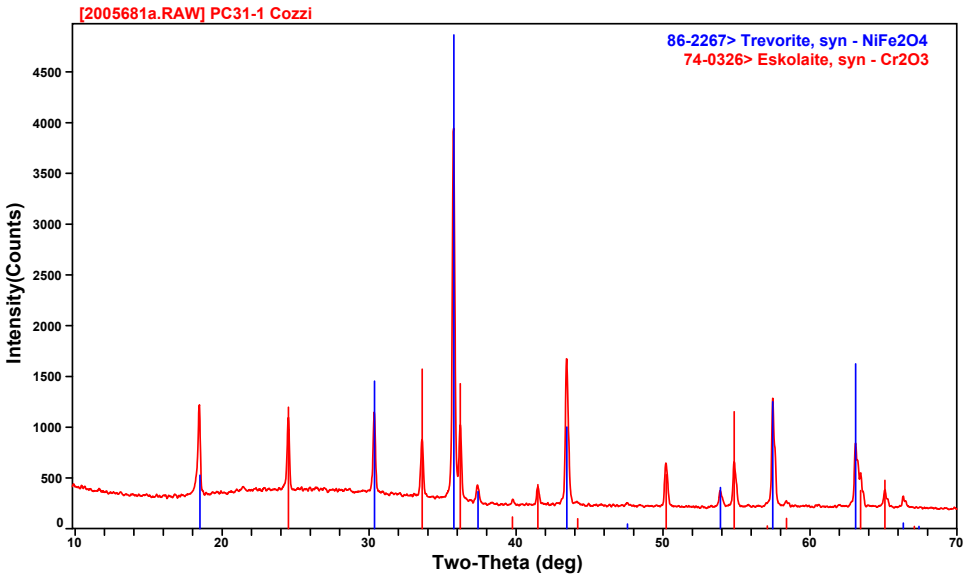


Figure 12. CXRD spectra of the insert glass sample (PC0031).

The XRD analysis of the upper pour spout bore sample (PC0006) indicated the presence of glass, spinel, and $RuO_2$ (see Figure 13). This is consistent with the chemical analyses of the upper pour spout bore sample containing 1.71 wt% $RuO_2$ compared to the pour stream glass (0.03 wt% $RuO_2$; Table IV) which is a 56% enrichment of $RuO_2$ (Table VII). Likewise, there is an 81% enrichment of $Rh_2O_3$ (Table VII). Therefore some mechanism is causing the $RuO_2$ and $Rh_2O_3$ to accumulate in the upper pour spout bore area over and above the amount of accumulation of the spinel forming components.

The spinel identified in the upper pour spout bore sample (PC0006) is a mixture of ~26 wt% trevorite ($NiFe_2O_4$) and ~8 wt% $NiCr_2O_4$ (see Table VI). The $Cr_2O_3$ is enriched in these deposits ~36X (Table V) relative to the amount in the pour stream sample (PC0033). Corrosion (oxidation) of the Inconel® 690 lining of the bore in this oxidizing environment on the pour spout is the most likely the primary source of the $Cr^{+3}$. Therefore, the molten glass and the Inconel® 690 pour spout lining are chemically interacting in this hot oxidizing environment. That is to say that the oxygen fugacity in the upper pour spout bore is more reducing than that of the insert (air $\log f_{O_2} = -0.68$) but considerably more reducing than that of the melt pool (melt pool $\log f_{O_2} = -5.5$). Therefore, the region of the upper pour spout bore experiences large gradients in both temperature and oxygen fugacity which can induce spinel crystallization, e.g. the measured activation energy for spinel crystallization in DWPF type waste glass in an oxidizing atmosphere ($\sum Fe^{+2}/Fe \sim 0$ at a $\log f_{O_2} = -0.68$ ) is 17.7 kcal/mole while the activation energy for spinel crystallization from a reducing glass ($\sum Fe^{+2}/Fe \sim 0.5$ at a $\log f_{O_2} = -7$) is only 2.9 kcal/mole [15]. Therefore, crystallization of spinel is more rapid in the oxidizing atmosphere of the upper pour spout bore and insert.

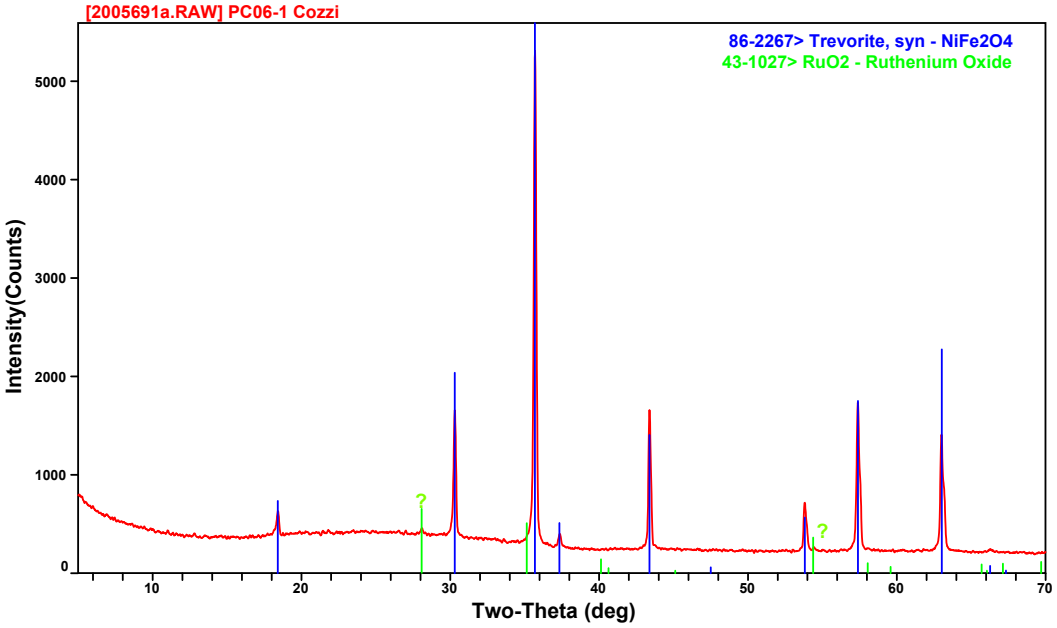


Figure 13. CXRD spectra of the upper pour stream bore sample (PC0006).

## 4.0 DISCUSSION

### 4.1 Pour Stream Sample

Visual observation of the pour stream sample (PC0033) showed the sample to be typical of a DWPF-type glass (opaque and reflective). Compositional analysis by ICP-ES demonstrated a correlation between the pour stream sample and the MFT batch 245. The MFT analysis predicted a glass viscosity within 2.5 poise of the pour stream sample calculated viscosity. The agreement between SME 245 and the pour stream sample was within ~10 poise. The MFT 245 analysis predicted a liquidus within 10ºC of the pour stream calculated liquidus. The SME and pour stream calculations for waste loading agree to within 0.35 wt%. The MFT and the pour stream calculations for waste loading agree to within 3.79 wt%. The measured REDOX was $Fe^{+2}/\Sigma Fe$ = 0.2 while the SME 245 target based on the {[F]-[3N]} correlation was 0.17 and the target based on the Electron Equivalents model was 0.15. Therefore, the viscosity [44], liquidus [1], and REDOX [55,56] models are all adequately controlling the DWPF glass properties.

It should be noted that SME 245 failed the Product Composition Control System (PCCS) Measurement Acceptable Region (MAR) as it had a calculated liquidus of 1029ºC and an acceptable MAR liquidus (accounting for analytic, model and measurement error) of 1017ºC for

the calculated liquidus. An engineering decision was made by DWPF to continue with processing of SME batch 245.

The pour stream sample, analyzed by X-ray diffraction in triplicate, contained no crystals and was totally amorphous even though the SME 245 failed the PCCS MAR. Therefore, there is no crystallization of spinel in the melt pool, which means that the liquidus model [1] is predicting and preventing melt pool crystallization. The amorphous nature of the pour stream sample (PC0033) is also in agreement with the recent work of Peeler et. al. [58] which validated the applicability of the liquidus model [1] to Sludge Batch 2 (SB2) Frit 320 melts in the waste loading range of 28-40 wt%.

It is important to distinguish between melt pool crystallization (volume crystallization) and surface crystallization as the liquidus model was developed to prevent catastrophic melt pool crystallization and not surface crystallization:

- *Surface crystallization* where crystal growth begins (i.e. nucleates) from the melt-atmosphere interface or the melt-container (melt-refractory) interface and grows perpendicular to the interface [59]

- *Volume crystallization* where crystal growth begins from either homogeneous or heterogeneous nucleation sites with a melt [59]
  - volume crystallization of the spinel primary liquidus phase has been shown to be heterogeneous forming on melt insolubles in the waste such as $RuO_2$ [16, 18]

Surface crystallization has not been considered to be problematic in nuclear waste glass melters since spinel precursors ($NaFe_2O_4$ [60,61] and $LiFe_2O_4$ [62]), which can redissolve in the melt pool have been found to form at the melt-atmosphere interface rather than insoluble $NiFe_2O_4$ spinels. Moreover, waste glass melts have been found to form a protective layer along the refractory walls which minimizes spinel formation in the melt pool from the refractory surfaces [63, 4], as long as the melt pool agitation or bubbling does not directly impinge on the melter walls.

Volume crystallization, on the other hand, can involve rapid nucleation of the melt pool. Once formed, the type of $NiFe_2O_4$ spinel crystals that occur in DWPF waste glass melts are refractory (reported melt temperature of 1660±10ºC [64]) and cannot be redissolved into the melt pool at the DWPF operating temperature of 1150ºC. Therefore, liquidus temperature modeling focused on heterogeneous volume crystallization rather than on surface crystallization [65].

## 4.2 Pour Spout Insert Sample

Compositional analysis of the insert sample (PC0031) revealed significantly greater quantities of transition elements (Cr, Fe, Mn, Ni, and Zn) and reduced amounts of other components (Al, Li, Na, Si) as compared to the pour stream sample. Indeed, the sample was enriched in $Cr_2O_3$ 141%

over the amount of $Cr_2O_3$ in the pour stream. CSEM analysis identified three distinct compositional regions (glass, spinels and a high chromium-containing phase). The CXRD analysis confirmed the presence of an amorphous phase, a spinel phase, and a chrome oxide phase. The $Cr_2O_3$ phase appeared in CSEM to form a coating or layer on the glass making it appear that the hot glass had chemically bonded to a $Cr_2O_3$ oxidized coating on the Inconel® 690 insert. A mass balance was performed based on the phases identified in CSEM and CXRD using the analyzed composition of PC0031 from Table IV. The $Li_2O$ content was used to assess the amount of glass present. The excess NiO (that over the amount present in the pour stream glass) was used to assess the amount of $NiFe_2O_4$ spinel present and the amount of excess $Cr_2O_3$ content was used to assess the amount of $Cr_2O_3$ in the deposits. The mass balance indicated that the sample was ~73 wt% glass, 16.4 wt% $NiFe_2O_4$, and 21 wt% $Cr_2O_3$ (see Table VI). However, some of the $Cr_2O_3$ and NiO enrichment in this sample could be present as $NiCr_2O_4$ which is isostructural with $NiFe_2O_4$ and indistinguishable on a CXRD spectra.

The pour spout insert sample was also enriched in Ru 10X over that present in the pour stream and also has a 17X enrichment in Rh. The Ru as $RuO_2$ and the Rh as $Rh_2O_3$ could be acting as nuclei for the crystallization of the 16.4 wt% $NiFe_2O_4$ spinel, but during CSEM no $RuO_2$ or $Rh_2O_3$ was observed to be associated with or acting as nuclei for the crystallization of $NiFe_2O_4$ spinel. The role of the $RuO_2$ and $Rh_2O_3$ is indeterminate although an intermediate oxide compound $RhCrO_3$, is known to occur [66]. In addition, if $RuO_2$ is reduced to Ru° locally contact with the Inconel® 690 alloy, there are known solid solutions between Ru° and Ni° [67].

### 4.3 Upper Pour Spout Bore Sample

The analysis of the pour spout bore sample is the most noteworthy sample examined. The compositional analysis of the upper pour spout bore sample (PC0006) revealed significantly greater quantities of transition elements and reduced amounts of other components (Al, Li, Na, Si) as compared to the pour stream sample. A mass balance was performed on this sample as was done for the previous two samples. The $Li_2O$ content was used to assess the amount of glass present. The excess NiO and $Fe_2O_3$ (the over the amount present in the pour stream glass) was used to assess the amount of $NiFe_2O_4$ spinel present and the amount of excess $Cr_2O_3$ content was used to assess the amount of $NiCr_2O_4$ in the deposits. The mass balance indicated that the sample was ~62 wt% glass, 25.8 wt% $NiFe_2O_4$, and 7.7 wt% $NiCr_2O_4$. In addition there was 1.71 wt% $RuO_2$ and 0.27 wt% $Rh_2O_3$ in these deposits which is a 56X and 81X increase of these components in the pour spout bore samples. The CSEM analysis identified a spinel phase enriched in Cr and glass. The CXRD analysis confirms the presence of an amorphous phase, a spinel phase, and $RuO_2$.

Known phase diagrams [68] indicate that $RuO_2$ can convert to Ru° and $Rh_2O_3$ to Rh° at $\log f_{O_2}$ =-5.5. However, the work of Schreiber [69] on SRL 131 glass indicates that $RuO_2$ is the stable phase in defense waste glass at all oxygen fugacities between $\log f_{O_2} = -0.68$ (air) and $\log f_{O_2} = -12$ at temperatures between 1000-1150°C. $RuO_2$ essentially consumes oxygen from other multivalent species in order to remain stable as $RuO_2$. This is confirmed by the CXRD

performed on sample PC0006 in this study, which showed the presence of $RuO_2$. Therefore some mechanism is causing the $RuO_2$ to accumulate in the upper pour spout bore area over and above the amount of accumulation of spinels and the associated transition metal species. The presence of all the $RuO_2$ and $Rh_2O_3$ indicates that the noble metals are agglomerating or reacting with the materials of construction in the riser in the region indicated in Figure 1 where there is constant contact of the melt stream with the Inconel® 690 during pouring.

# 5.0 POTENTIAL MECHANISMS FOR ACCUMULATION OF MELTER DEPOSITS IN THE DWPF POUR SPOUT

## 5.1 Gradients in Temperature and Oxygen Fugacity

The DWPF liquidus model was developed to prevent volume crystallization of the melt pool at the normal melter operational temperatures, e.g. between 1050-1150°C, at normal oxygen fugacities experienced in waste glass melters, e.g. between $\log f_{O_2}$ = -2 and $\log f_{O_2}$ = –9.

Operation of the SGM melter, specifically SGM Campaign 6, at waste loadings in excess of 38 wt% (Table III), e.g. in the range in which DWPF experienced severe pour spout crystallization, is achievable if the pour spout is well insulated and kept hot.

As the glass flows up the riser, down the pour spout, and over the pour spout insert the following occurs:

- cooler temperatures are encountered, e.g. <1050°C which is below the liquidus of the glass being poured which enhances the kinetics of crystallization of spinel
- more oxidizing atmospheres (fugacities) are encountered, e.g. air $\log f_{O_2}$ = –0.68 which enhances the kinetics of the crystallization of spinel [15] relative to the reducing atmosphere of the melt pool
- cooler Inconel® 690 surfaces are contacted that act as heat sinks inducing surface crystallization instead of bulk or volume crystallization
- cooler Inconel® 690 surfaces are contacted that are themselves being oxidized due to exposure to air and these surfaces release $Cr_2O_3$, which can nucleate spinels

Such crystallization in the melter riser, specifically in the tip of the pour spout channel had been observed during the first campaign of the DWPF pilot Scale Glass Melter (SGM). Crystallized deposits formed on ten separate occasions and were attributed to the fact that the tip of the pour spout channel lacked sufficient insulation which caused this region to be significantly cooler, ~800°C, than the thermocouples were indicating. Additional insulation and relocation of the thermocouples remediated the pluggage difficulties.

If the DWPF pour spout insert and upper pour spout bore are cooler than the liquidus temperature predicted by the DWPF Product Composition Control System (PCCS), e.g. a liquidus temperature of 987°C predicted for MFT 245 (Table IV) and a liquidus of 997°C

predicted from the pour stream analysis (Table IV), then surface nucleation of crystals on these cooler surfaces is more likely to occur. This is because a higher waste loaded melt is closer to its crystallization temperature when it exits the melter than a lower waste loaded melt. Thus, unless a higher waste loaded melt is moved through the cooler region very rapidly, the glass crystallizes instead of "undercooling" to an amorphous state. In other words, the riser temperature profile is too steep (the bore is not hot enough) which allows spinels to form at higher waste loadings because the cooling rate is not fast enough in this region.

### 5.1.1 Heat Sink Induced Crystallization

Because glass is a supercooled liquid it exhibits a phenomena known as "undercooling" (see Figure 14). On cooling a liquid from the initial state of A (melt temperature), the volume will decrease steadily along line AB. If the rate of cooling is too slow, e.g. if the DWPF riser temperatures are too low, and nuclei are present, crystallization will take place at the freezing temperature ($T_f$). The volume will decrease sharply from B to C; thereafter, the solid will continue to crystallize and contract along line CD. If the rate of cooling is sufficiently rapid, e.g. if the DWPF riser temperatures are sufficient, crystallization will not take place at $T_f$ and the volume of the supercooled liquid continues to decrease along line BE which is a continuation of line AB. Once the temperature falls below point E (the glass transition temperature, $T_g$) the supercooled liquid is deemed a "glass." Therefore, the temperature profile within the DWPF riser is of critical importance as to whether or not crystals will form in this region of the pour spout due to undercooling.

In order to demonstrate the importance of cooling rate, dT/dt (where T is temperature in °C and t is time in seconds) calculations were performed assuming different temperatures for the upper pour spout bore ranging from 1150°C to 900°C. The equation for the lowering of temperature with time for a finite body in contact with a heat sink (substrate) at a lower temperature may be written as follows [70]

$$\frac{T_t - T_s}{T_{t=0} - T_s} = \exp\left(t\left(\frac{K_m}{\rho \bullet C_p}\right)d^2\right) \qquad (1)$$

where $T_t$ = temperature at time t (°C)
$T_s$ = temperature of the substrate (°C)
$K_m$ = thermal conductivity at the melting point (cal/cm sec °C)
$C_p$ = specific heat (cal/g °C)
d = thickness (or radius if the cooling body is spherical) in cm
$\rho$ = density in g/cm$^3$ at the melt temperature

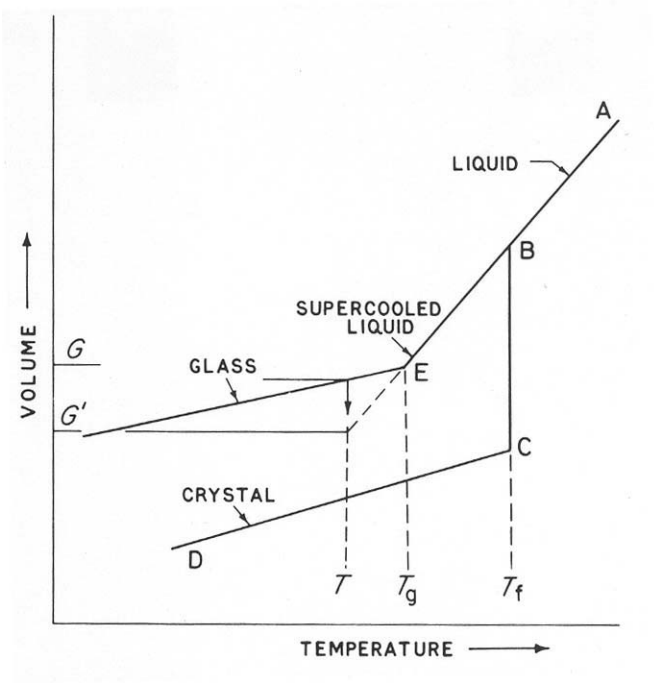


Figure 14. Relationship between the glassy, liquid and solid states (from Reference 59).

Since DWPF glasses undergo Newtonian cooling, the term hd can be substituted for $K_m$ where h is the heat transfer coefficient. Taking the logarithms of Equation 1 and differentiating with respect to t, the following expression for an instantaneous cooling rate (Q):

Equation 2
$$Q \equiv \frac{dT}{dt} = (T_t - T_s)\left(\frac{h}{\rho \bullet C_p}\right)d$$

where h = heat transfer coefficient (cal/cm$^2$ sec °C)

Note that the latent heat of fusion ($\Delta H_f$) does not enter the calculation since crystallization only intervenes when the cooling rate is not great enough to prevent diffusional ordering from occurring [70].

The following parameters were used to approximate h, ρ, d, $T_t$, $T_s$, and $C_p$ for DWPF type glass:

- radius of the DWPF pour stream ~0.25 cm
- $T_t = T_L$ (°C)
- $T_s$ = varied from 900°C to 1150°C
- $\rho = 2.47$ g/m$^3$ for a high-Fe 131 glass [71,72] which is similar to the measured room temperature density in this report of 2.503 g/cm$^3$
- $C_p$ = specific heat at $T_s$ for a high-Fe 165 glass [73] which is similar to a high-Fe Frit 320 glass
- h = 1.7 cal/cm$^2$sec°C valid for SRL 131/Stage 1 waste glass above 900°C [74].

This allows $Q \equiv dT/dt$, a critical cooling rate to avoid crystallization to be estimated for DWPF glasses depending on the temperature of the Inconel® 690 substrate. This calculation is only approximate but serves to illustrate how much more rapidly the glass must be cooled as the Inconel® 690 substrate temperatures decrease, e.g. as the $\Delta T \equiv T_L - Ts$, the degree of undercooling, increases. For example, at the liquidus temperature of 997°C for the DWPF pour spout sample PC0003 analyzed in this report (see Table IV) the relation between Q and the temperature of the substrate (heat sink) is:

Equation 3 Temperature of Heat Sink(°C) = 998.00613 - 1.8619 dT/dt (deg C/sec)

At a heat sink (pour spout) temperature of 980°C (the temperature of the pour spout tip near the disengagement point for SGM-1 from reference 13), a cooling rate of ~+9.7°C/sec is needed to prevent crystallization. At the pour spout bore temperature of SGM-1, e.g. 1040°C [13], a cooling rate of <1°C/sec is needed to prevent crystallization. If the pour spout were hotter, e.g. 1100°C then a slower cooling rates are needed to prevent crystallization. This latter substrate temperature is consistent with the riser and pour spout temperatures reported during the 5$^{th}$ campaign of the LSFM melter, e.g. in the range of 1125°C ± 10°C and 1075°C ± 10°C, respectively, when no pour spout pluggages were observed [9].

If the liquidus temperature of the glasses being poured were higher, e.g. 1050°C, then the relation between Q and the temperature of the substrate is:

Equation 4 Temperature of Heat Sink = 1050.9779 - 1.8471 dT/dt (deg C/sec)

For a melt with a liquidus of 1050°C, the cooling rates necessary to prevent crystallization at 980°C, 1040°C, and 1100°C become higher, e.g. 38°C/sec, +6°C/sec and <1°C/sec, respectively. So more rapid cooling rates are necessary for the same substrate temperatures at higher waste loadings when the liquidus temperatures are higher. This can also be stated as more rapid cooling rates are necessary for larger undercoolings (ΔT), e.g. larger differences between $T_L$ and $T_s$. It should also be noted that the larger the undercooling the more rapid the nucleation rate in glasses [75].

This suggests that if the DWPF pour spout bore or insert region is not sufficiently hot enough, e.g. the higher waste loaded glasses may be cooling off too slowly, e.g. the degree of undercooling is too great, which allows surface nucleation of spinels on the inside of the upper bore. This in conjunction with the more rapid nucleation of spinels in oxidizing environments and the availability of excess $Cr_2O_3$ from Inconel® 690 oxidation has led to increased deposition in the spout and insert. This is consistent with the operating history of the LSFM which had a pour spout temperature of ~1075°C, poured lower waste loaded glasses, and did not have any pour spout pluggages. It is also consistent with the hotter spout designed for SGM after the 10 pour spout pluggages experienced when the pour spout tip was 980°C. Once the SGM was redesigned, it was able to pour glasses with calculated waste loadings up to ~42 wt% (see Figure 15 and Figure 16 which have the DWPF samples analyzed in this study superimposed). It should also be noted that the current DWPF melts have calculated viscosities in the range of the glasses melted during SGM 6-6 (Figure 17).

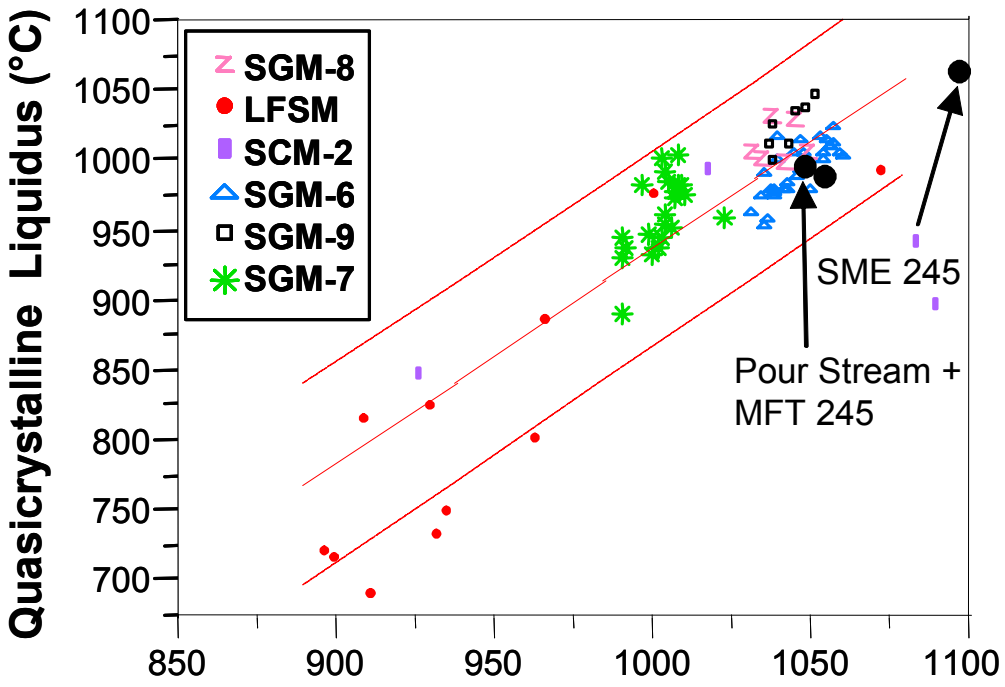


Figure 15 Comparison of the liquidus temperatures for various pilot scale melters compared to the samples analyzed in this study (solid black circles).

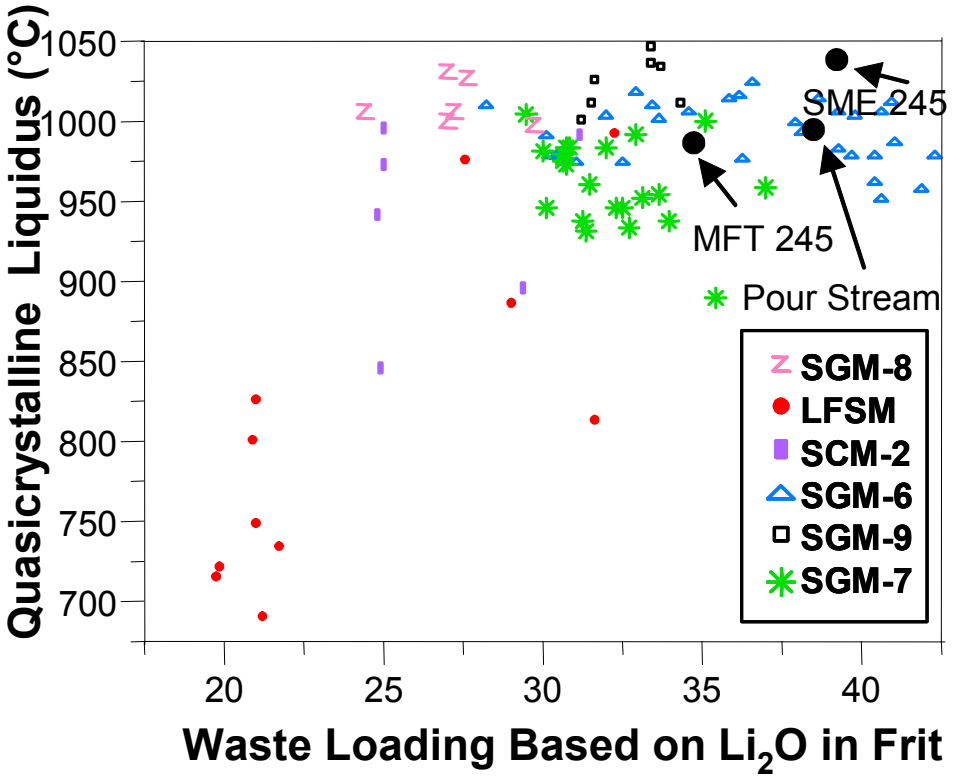


Figure 16 Comparison of the liquidus temperatures and waste loading for various pilot scale melters compared to the samples analyzed in this study (solid black circles).

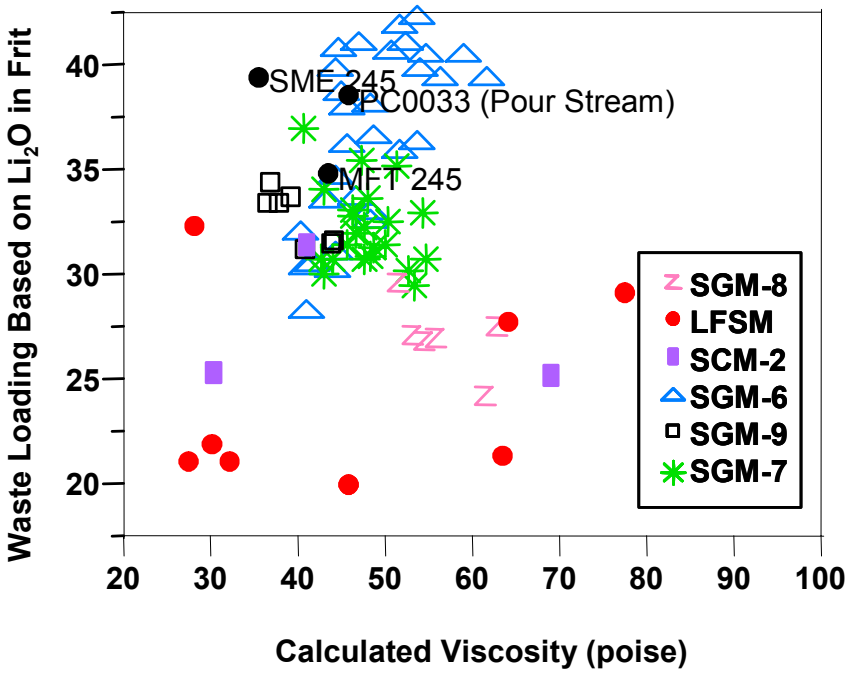


Figure 17. Comparison of the calculated viscosities and waste loadings for various pilot scale melters compared to the samples analyzed in this study (solid black circles).

### 5.1.2 Inconel® 690 Oxidation and Induced Crystallization

Oxidation of Inconel® 690 to $Cr_2O_3$ rich oxide is evidenced by the mass balance of the pour spout insert samples analyzed in this report, e.g. the sample was ~73 wt% glass, 16.4 wt% $NiFe_2O_4$, and 21 wt% $Cr_2O_3$. At the temperature of the pour spout insert, and indeed anywhere between 800-1100°C, Inconel® 690 can rapidly oxidize to form a protective chrome oxide layer [76,77] even in the presence of $Fe_2O_3$ and FeO [78]. Recalling that $\log f_{O_2}$ =-5.5 for DWPF glass at a $Fe^{+2}/\Sigma Fe$ ratio=0.2, it should be noted that at oxygen fugacities more positive than $\log f_{O_2}$ = -10, Ni-rich alloys decompose to $NiCr_2O_4$ and NiO [77]. This "free" NiO further complexes with the $Fe_2O_3$ in DWPF glass forming $NiFe_2O_4$ which depletes the Inconel® 690 in NiO leaving an enrichment in $Cr_2O_3$ deposits. This is evidenced by the relative positions of the Inconel® 690 alloy composition (point A) to the insert deposit composition (point C) shown in Figure 18 in mol percentage of Cr and Ni. Path AC in Figure 18 indicates that the deposits form by oxidation of Inconel® 690 and NiO depletion.

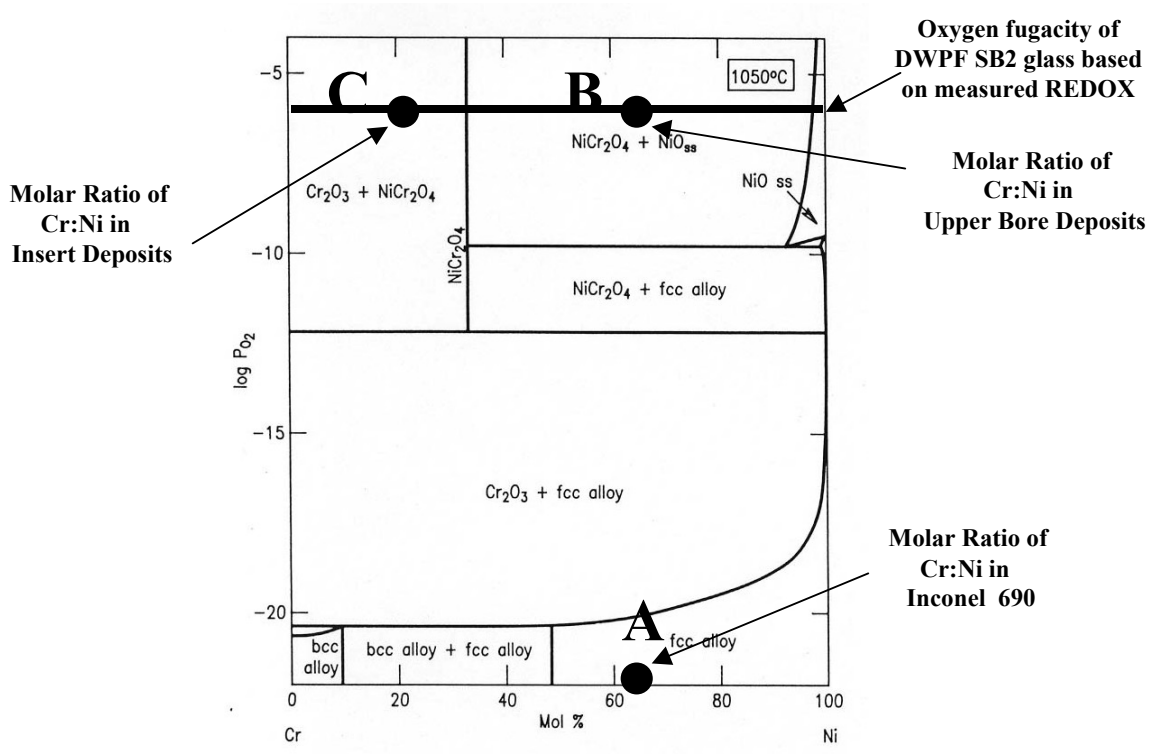


Figure 18. Binary phase diagram at 1050°C demonstrating the phases that are formed upon oxidation of a Ni-Cr alloy like Inconel® 690 [77].

The mass balance of the upper pour spout bore sample also indicated that the sample was $Cr_2O_3$ enriched, e.g. ~62 wt% glass, 25.8 wt% $NiFe_2O_4$, and 8 wt% $NiCr_2O_4$. Figure 18 readily shows that the Ni:Cr mole percentage of Inconel® 690 (point A) is the same as the ratio in the upper pour spout bore deposits (point B). Recalling that $\log f_{O_2}$ =-5.5 for DWPF glass at a $Fe^{+2}/\Sigma Fe$ ratio=0.2, it should be noted that at oxygen fugacities more positive than $\log f_{O_2}$ = -10, Ni-rich alloys decompose to $NiCr_2O_4$ and NiO [77]. This "free" NiO further complexes with the $Fe_2O_3$ in DWPF glass forming $NiFe_2O_4$, These are the two main spinel components determined to be in the upper pour spout bore by mass balance (see Table V). This is evidenced by the relative positions of the Inconel® 690 alloy composition to the upper pour spout bore deposit composition to the insert deposit composition shown in Figure 18. These compositions represent the molar percentages of Cr and Ni in the deposits and in the alloy and indicate that the deposits form by oxidation of Inconel® 690 (path AB in Figure 18).

Corrosion of the Inconel® 690 may be enhanced by higher concentrations of $Fe_2O_3$ in DWPF glass at the higher waste loadings being processed. The higher $Fe_2O_3$ content could be acting as a diffusion driver for reaction with Ni from the Inconel® 690 which gets converted to NiO in the oxidizing environment of the upper bore. Corrosion of the Inconel® 690 in the upper bore also appears to be enhanced by the higher concentration of noble metals in SB2. The noble metals did not appear to be nucleating the spinel phases based on the CSEM analyses performed in this study. It is possible that the noble metals are being reduced to their elemental form at the

interface with the alloy Inconel® 690 where known Ni°-Ru° solid solutions could form or galvanic corrosion prior to reoxidation of the Ni° and Ru° to the oxides NiO and $RuO_2$. Further investigation of the stability of Inconel® 690 in higher noble metal feeds in reduced glasses is needed.

### 5.2 Elevated $Cr_2O_3$ in the Pour Stream

The pour stream sample was analyzed to have elevated $Cr_2O_3$ over the amounts reported in SME-245 and MFT-245. The $Cr_2O_3$ is 20% higher in the pour stream than in the SME-245 analyses and 37% higher than in the MFT-245 analyses (based on the data in Table V). One of the three replicate samples used to determine the average 0.15 wt% $Cr_2O_3$ in the pour stream sample was as high as 0.25 wt%. Therefore, the apparent elevation of $Cr_2O_3$ in the pour stream sample may be analytic variation or it may mean that the glass is reacting with the K-3 refractory or the Inconel® 690 DWPF materials of construction. Elevated $Cr_2O_3$ in the pour stream will raise the liquidus temperature of the glass and the nucleation frequency will be greater at higher undercoolings as discussed in Section 4.1.1.

The K-3 refractory has a high $Cr_2O_3$ content. K-3 refractory corrosion occurs because a spinel phase, $MgAlCrO_4$ in the K-3 refractory reacts with $Fe_2O_3$, NiO, and $SiO_2$ in the DWPF glass to form $NiCrFeO_4$ spinels (a mixture of $NiFe_2O_4$ and $NiCr_2O_4$ spinels) and a magnesium aluminosilicate phase known as krinovite [63]. The spinel and krinovite reaction products were found in the bottom of the IDMS melter after 7 years of continuous operation co-located with downward bores of pockets of elevated noble metals [20, 22]. There is some evidence of MgO enhancement (~16% based on the data in Table V) in the pour stream sample over that analyzed in the MFT-245 that may support this hypothesis, but the MgO released by the K-3 refractory may also be consumed in the formation of the krinovite phase.

In 1997 GTS Duratek experienced significant corrosion of K-3 refractory in the SRS M-Area melter, which was indicated by elevated Cr in the pour stream glass (the M-Area waste contained only the 0.006-0.03 wt% $Cr_2O_3$ [79]). The elevated $Cr_2O_3$ levels they experienced in their melt were only ~0.1 to 0.2 wt%. Upon adding a combination of MgO (~1 wt%) and other spinel formers to their frit components, the K-3 corrosion was mitigated. GTS Duratek attributed the reduction in $Cr_2O_3$ in the pour stream to the formation of a protective glass/spinel layer on the K-3 refractory. Since frits at SRS have always contained between 1-2 wt% MgO primarily to enhance glass durability, the attack of the K-3 refractory has never been observed. As early as the SRS 1941 project melter experience [4] the DWPF glasses were always found to form a protective glass/spinel layer on the K-3 refractory, presumably because SRS glass formulations always contained MgO. Recent frit formulations, e.g. Frit 320, do not contain MgO although SB2 and the Tank 40 glass and the SME-245 and MFT-245 analyses all demonstrate that at least 1 wt% MgO is present in the SB2 glass currently being melted by DWPF. The study of K-3 corrosion in the presence and absence of MgO needs to be further examined before any conclusions can be drawn.

## 6.0 CONCLUSIONS

The Defense Waste Processing Facility (DWPF) Engineering requested characterization of three glass samples that were taken from Melter #2 after the waste loading had been increased, e.g. after the new quasicrystalline liquidus model had been implemented and after DWPF switched from processing with Frit 200 to Frit 320. These samples were taken after DWPF observed very rapid buildup of deposits in the upper pour spout bore and on the pour spout insert while processing the high waste loading (~38 wt% feedstock). Rapid deposition in these locations had not occurred prior to this and, in turn, stopped after waste loading decreased. This buildup in the spout is believed to have contributed to pour stream instability. These samples were evaluated at SRTC using various analytical techniques for potential impacts on pouring problems recently experienced by the DWPF.

The pour stream sample was determined to be homogenous, amorphous, and representative of SME/MFT batch 245. The calculated viscosity from the pour stream analysis was within 2.5 poise of the MFT-245 Product Composition Control System (PCCS) prediction. The calculated liquidus from the pour stream analysis was within 10°C of the MFT-245 PCCS prediction. The glass REDOX was within 0.03 of the target and the waste loading (based on the reported $Li_2O$) was within 3.8 wt% of the MFT-245 target. This indicated that the viscosity, liquidus, and REDOX models are keeping DWPF processing in control. There was no crystallization observed in the pour stream sample.

The most likely mechanism by which the severe crystallization of the pour spout and insert occurred are the temperature and oxygen fugacity (oxidation) profiles of the DWPF pour spout in conjunction with the higher waste loadings. The DWPF liquidus model was developed to prevent volume crystallization of the melt pool at the normal melt pool temperatures, e.g. between 1050-1150°C, and at the normal oxygen fugacities experienced in waste glass melters, e.g. between $\log f_{O_2}$ = -2 ($Fe^{+2}/\Sigma Fe$=0.09) and $\log f_{O_2}$ = –9 ($Fe^{+2}/\Sigma Fe$=0.33). Operation of the SGM melter, specifically SGM Campaign 6, at waste loadings in excess of 38 wt% (Table III), e.g. in the range in which DWPF experienced severe pour spout crystallization, is achievable if the pour spout is well insulated and kept hot.

In the DWPF pour spout the glass flows up the riser, down the pour spout, and over the pour spout insert. During this path the following occurs:

- cooler temperatures are encountered, e.g. <1050°C which is below the liquidus of the glass being poured which initiates crystallization of spinel
- more oxidizing atmospheres (fugacities) are encountered, e.g. air $\log f_{O_2}$ = –0.68 which enhances the kinetics of the crystallization of spinel [15] relative to the reducing atmosphere of the melt pool ($\log f_{O_2}$ = –5.5)
- cooler Inconel® 690 surfaces are contacted that act as heat sinks inducing surface crystallization instead of bulk or volume crystallization
- cooler Inconel® 690 surfaces are contacted that are themselves being oxidized due to exposure to air and these surfaces release $Cr_2O_3$, which can nucleate spinels

Such crystallization in the melter riser, specifically in the tip of the pour spout channel had been observed during the first campaign of the DWPF pilot Scale Glass Melter (SGM). Crystallized deposits formed on ten separate occasions and were attributed to the fact that the tip of the pour spout channel lacked sufficient insulation which caused this region to be significantly cooler, ~800°C, than the thermocouples were indicating. Additional insulation and relocation of the thermocouples remediated the pluggage difficulties.

If the DWPF pour spout insert and upper pour spout bore are cooler than the liquidus temperature predicted by the DWPF Product Composition Control System (PCCS), e.g. a liquidus temperature of 987°C predicted for MFT 245 (Table IV) and a liquidus of 997°C predicted from the pour stream analysis (Table IV), then surface nucleation of crystals on these cooler surfaces is more likely to occur. This is because a higher waste loaded melt is closer to its crystallization temperature when it exits the melter than a lower waste loaded melt. Thus, unless a higher waste loaded melt is moved through the cooler region very rapidly, the glass crystallizes instead of "undercooling" to an amorphous state. In other words, the riser temperature profile is too steep (the bore is not hot enough) which allows spinels to form at higher waste loadings because the cooling rate is not fast enough in this region.

This is supported by the analyses performed in this study. The mass balance of the pour spout insert samples indicated that the sample was ~73 wt% glass, 16.4 wt% $NiFe_2O_4$, and 21 wt% $Cr_2O_3$. At the temperature of the pour spout insert, Inconel® 690 has been found to rapidly oxidize to form a protective chrome oxide layer. Ni-rich alloys such as Inconel® 690 oxidize to $NiCr_2O_4$ and NiO. This "free" NiO further complexes with the $Fe_2O_3$ in DWPF glass forming $NiFe_2O_4$ which depletes the Inconel® 690 in NiO leaving an enrichment in $Cr_2O_3$ deposits. Which is the most likely mechanism for the accumulation of deposits on the pour spout insert.

Likewise, in the upper pour spout bore, Inconel® 690 can oxidize to $NiCr_2O_4$ and NiO. The latter reacts with $Fe_2O_3$ in DWPF glass forming $NiFe_2O_4$. The presence of $NiCr_2O_4$ (~8 wt%) and $NiFe_2O_4$ (~26 wt%) in the upper bore sample confirms that this mechanism is operable. Corrosion (oxidation) of Inconel® 690 in the DWPF riser, bore, and insert can be enhanced by the following:

- higher concentrations of $Fe_2O_3$ in DWPF glass at the higher waste loadings being processed where the $Fe_2O_3$ content could be acting as a diffusion driver for reaction with Ni from the Inconel® 690

- higher concentrations of noble metals in SB2 accelerating Inconel® 690 corrosion

Knowing that the DWPF pour spout bore and insert regions are more oxidizing than the melt pool and not sufficiently hot enough allows higher waste loaded glasses to cool too slowly. In other words, the degree of undercooling is too great, and the surface nucleation of spinels on the inside of the upper bore, spout, and insert can occur. The surface nucleation of spinels in the cooler more oxidizing regions of the pour spout is further enhanced in oxidizing environments

because the activation energy of spinel nucleation is more rapid (17.7 kcal/mole) than in reducing environments (2.9 kcal/mole). In addition, the oxidative corrosion of Inconel® 690 provides excess $Cr_2O_3$ nuclei that can act as heterogeneous nuclei for spinel growth. The oxidative corrosion of Inconel® 690 and the insufficient heat in the pour spout mechanism is consistent with the operating history of the LSFM which had a pour spout temperature of ~1075°C, poured lower waste loaded glasses, and did not experience any pour spout pluggages. The oxidative corrosion of Inconel® 690 and the insufficient heat in the pour spout mechanism is also consistent with the pour spout pluggages experienced during SGM-1 when the pour spout tip was 980°C. Once the SGM-1 pour spout was better insulated and the thermocouple locations redesigned, the SGM was able to pour glasses with calculated waste loadings up to ~42 wt%, e.g. SGM 6-6.

One other observation noted in this study was elevated $Cr_2O_3$ in the pour stream over that analyzed in the SME and MFT may indicate one of the following:

- analytic error
- K-3 refractory corrosion due to lack of MgO in the Frit 320 formulation although SB 2 contains sufficient MgO that this should not be a problem
- oxidation of the Inconel® 690 in the riser

Elevated $Cr_2O_3$ in the pour stream will raise the liquidus temperature of the glass and the nucleation frequency will be greater at higher undercoolings as discussed in Section 5.1.1.

## 7.0 RECOMMENDATIONS

- Study the corrosion of Inconel® 690 in the presence of higher $Fe_2O_3$ containing (higher waste loaded glasses) in reduced melts, e.g. at an $Fe^{+2}/\Sigma Fe$ ratio of 0.2
- Study the corrosion of Inconel® 690 in the presence of noble metals at a $Fe^{+2}/\Sigma Fe$ ratio of 0.2
- Measure the temperature of the upper bore
  - initiate measures to increase the heat in the pour spout upper bore and insert region
- Measure the corrosivity of K-3 refractory under reduced conditions in the presence and absence of MgO in the frit

## 8.0 REFERENCES


1 K.G. Brown, C.M. Jantzen and G. Ritzhaupt, **"Relating Liquidus Temperature to Composition for Defense Waste Processing Facility (DWPF) Process Control,"** WSRC-TR-2001-00520, Westinghouse Savannah River Co., Aiken, SC (October, 2001).

2 D.C.Iverson to C.M. Jantzen and S.L. Marra, **"Melter 2 Samples,"** e-mail dated October 13, 2003.

3 M.J. Plodinec, **"Long-Term Waste Management Progress Report Small-Scale Electric Meter, IV. Effects of Feed Mixing and Segregation on Glass Melting,"** U.S. DOE Report DPST-79-227, E.I. duPont deNemours & Co., Savannah River Laboratory, Aiken, SC (January, 1979).

4 W.N. Rankin, P.E. O'Rourke, P.D. Soper, M.B. Cosper, and B.C. Osgood, **"Evaluation of Corrosion and Deposition in the 1941 Melter,"** U.S. DOE Report DPST-82-231, E.I. duPont deNemours & Co., Savannah River Laboratory, Aiken, SC (March, 1982).

5 T.L. Allen, D.C. Iverson, and M.J. Plodinec, **"History of the Small Cylindrical Melter,"** U.S. DOE Repot DP-1676, E. I. duPont deNemours &Co., Aiken, SC (August 1985).

6 M.J. Plodinec and K.R. Routt, **"Performance of Structural and Active Components of the Small-Scale Cylindrical Melter: First Operating Campaign,"** U.S. DOE Report DPST-80-494, E. I. duPont deNemours &Co., Aiken, SC (July 18, 1980).

7 K.R. Routt, M.J. Plodinec, and M.A. Porter, **"Performance of Structural and Active Components of the Small Cylindrical Melter: Second Operating Campaign,"** U.S. DOE Report DPST-80-654, E. I. duPont deNemours &Co., Aiken, SC (December 1, 1980).

8 D.C. Iverson and D.F. Bickford, **"Evaluation of Materials Performance in a Large-Scale Glass Melter After Two Years of Vitrifying Simulated SRP Defense Waste,"** Sci. Basis for Nuclear Waste Management, VIII, Materials Research Society, Pittsburgh, PA, 839-845 (1985).

9 W.P. Colven, D.M. Sabatino, J.L. Kessler, H.C. Wolf, **"Summary of the Fifth Run of the Large Slurry-Fed Melter,"** U.S. DOE Report DPST-82-890, E.I. duPont deNemours & Co., Savannah River Laboratory, Aiken, SC (September, 1984).

10 C.M. Jantzen, **"Lack of Slag Formation in the Scale Glass Melter,"** U.S. DOE Report DPST-87-373, E.I. duPont deNemours & Co., Savannah River Laboratory, Aiken, SC (April, 1987).

11 M.R. Baron and M.E. Smith, **"Summary of the Drain and Restart of the DWPF Scale Glass Melter, "** U.S. DOE Report DPST-88-481, E.I. duPont deNemours & Co., Savannah River Laboratory, Aiken, SC (May, 1988).

12 A.F. Weisman/Scale Melter Team, **"Run Summaries from SGM-1, SGM-3, and SGM-4,"** U.S. DOE Report DPST-86-862, E.I. duPont deNemours & Co. Savannah River Laboratory, Aiken, SC (1986).

13 A.F. Weisman, J.L. Mahoney, M. Rodman, K.R. Crow, D.M. Sabatino, and G.A. Griffin, **"Scale Melter Startup Review,"** U.S. DOE Report DPST-86-361, E.I. duPont deNemours & Co., Savannah River Laboratory, Aiken, SC (April, 1986).

14 C.M. Jantzen, **"Devitrification of Scale Melter Glass in Riser Heater,"** U.S. DOE Report DPST-86-461, E.I. duPont deNemours & Co., Savannah River Laboratory, Aiken, SC (May, 1986).

15 C.M. Jantzen, D.F. Bickford, and D.G. Karraker, **"Time-Temperature Transformation Kinetics in SRL Waste Glass,"** Advances in Ceramics, 8, American Ceramic Society, Westerville, OH, 30-38 (1984).

16 D.F. Bickford and C.M. Jantzen, **"Devitrification of SRL Defense Waste Glass**," Scientific Basis for Nuclear Waste Management, VII, G.L. McVay (Ed.), Elsevier Publ, New York, 557-565 (1984).

17 C.M. Jantzen and D.F. Bickford, **"Leaching of Devitrified Glass Containing Simulated SRP Nuclear Waste,"** Scientific Basis for Nuclear Waste Managment, VIII, C.M.Jantzen, J.A. Stone, and R.C. Ewing (Eds.), Materials Research Society, Pittsburgh, PA, 135-146 (1985).

18 D.F. Bickford and C.M. Jantzen, **"Devitrification of Defense Nuclear Waste Glasses: Role of Melt Insolubles,"** J. Non-Crystalline Solids, 84, 299-307 (1984).

19 S.L. Marra, M.K. Andrews, and C.A. Cicero, **"Time-Temperature-Transformation Diagrams for DWPF Projected Glass Compositions,"** Proceedings of the Environmental and Waste Management Issues in the Ceramic Industry, G.B. Mellinger (Ed.), Ceramic Transactions, V. 39, Am. Ceram. Soc., Westerville, OH, 283-302 (1994).

20 C.M. Jantzen and D.P. Lambert, **"Inspection and Analysis of the Integrated DWPF Melter System (IDMS) After Seven Years of Operation,"** U.S. DOE Report WSRC-RP-575, Westinghouse Savannah River Co., Aiken, SC (February, 1997).

21 M.E. Smith, N.D. Hutson, D.H. Miller, J. Morrison, H. Shah, J.A. Shuford, J. Glasscock, F.H. Wurvinger, and J.R. Zamecnik, **"Checkout and Startup of the Integrated DWPF Melter System,"** U.S. DOE Report WSRC-RP-89-321, Westinghouse Savannah River Co., Savannah River Laboratory, Aiken, SC (November, 1989).

22 C.M. Jantzen and D.P. Lambert, **"Inspection and Analysis of the Integrated DWPF Melter System (IDMS) after Seven Years of Continuous Operation,"** Environmental

Issues and Waste Management Technologies in the Ceramic and Nuclear Industries, V, G. T. Chandler (Eds.), Ceramic Transactions, V. 107, 653-661 (2000).

23 M.K. Andrews and J.R. Harbour, **"Chromium Levels in Feed and Glass for DWPF Startup Melter Campaigns,"** U.S. DOE Report WSRC-TR-95-0368, Westinghouse Savannah River Company, Aiken, SC (September, 1995).

24 J.P. Moseley, **"Summary of the First Run of the Large Slurry-Fed Melter,"** U.S. DOE Report DPST-82-461, E.I. duPont deNemours & Co., Savannah River Laboratory, Aiken, SC (April, 1982).

25 D.M. Sabatino, H.C. Wolf and J.P. Mosley, **"Summary of the Second Run of the Large Slurry-Fed Melter,"** U.S. DOE Report DPST-82-624, E.I. duPont deNemours & Co., Savannah River Laboratory, Aiken, SC (July, 1982).

26 D.P. Lewis **"Third Run of the Large Slurry-Fed Melter (LSFM-3),"** U.S. DOE Report DPST-83-905, E.I. duPont deNemours & Co., Savannah River Laboratory, Aiken, SC (June, 1983).

27 H.C. Wolf, W.P. COlven, D.M. Sabatino, and J.P. Mosley, **"Summary of the Fourth Run of the Large Slurry-Fed Melter,"** U.S. DOE Report DPST-82-9111, E.I. duPont deNemours & Co., Savannah River Laboratory, Aiken, SC (August 1982).

28 J.L. Kessler, D.M. Sabatino, W.P. Colven, **"Summary of the Sixth Run of the Large Slurry-Fed Melter,"** U.S. DOE Report DPST-83-306, E.I. duPont deNemours & Co., Savannah River Laboratory, Aiken, SC (March, 1983).

29 W.P. Colven, D.M. Sabatino, J.L. Kessler, **"Summary of the Seventh Run of the Large Slurry-Fed Melter,"** U.S. DOE Report DPST-83-692, E.I. duPont deNemours & Co., Savannah River Laboratory, Aiken, SC (July, 1983).

30 D.M. Sabatino, J.L. Kessler, and W.P. Colven, **"Summary of the Eighth Run of the Large Slurry-Fed Melter,"** U.S. DOE Report DPST-83-915, E.I. duPont deNemours & Co., Savannah River Laboratory, Aiken, SC (October, 1983).

31 J.L. Kessler, **"Melter Summary of the Ninth Run of the Large Slurry Fed Melter,"** U.S. DOE Report DPST-83-740, E.I. duPont deNemours & Co., Savannah River Laboratory, Aiken, SC (September, 1983).

32 D.M. Sabatino, W.P. Colven, D.C. Iverson, **"Summary of the Tenth Run of the Large Slurry-Fed Melter,"** U.S. DOE Report DPST-84-255, E.I. duPont deNemours & Co., Savannah River Laboratory, Aiken, SC (October, 1984).

33 K.R. Crow, A.F. Weisman, P.D. Guidotti, A.M. Wehner, G.A. Griffin, J.M. Micallef, J.M. O'Rourke, M. Yoshioka, **"Summary of Campaigns SGM-4 and SGM-5 of the DWPF**

**Scale Glass Melter,"** U.S. DOE Report DPST-87-247, E.I. duPont deNemours & Co., Savannah River Laboratory, Aiken, SC (1987).

34 P.D. Guidotti, K.R. Crow, A.F. Weisman, M.R. Baron, A.M. Wehner, J.A. Voogd, M.E. Smith, S.L. Goudelock, G.A. Griffin, J.A. Shuford, J.M. O'Rourke, "**Summary of Campaigns SGM-6 and SGM-7 of the DWPF Scale Glass Melter,"** U.S. DOE Report DPST-87-532, E.I. duPont deNemours & Co. Savannah River Laboratory, Aiken, SC (1987).

35 R.E. Edwards, S.L. Goudelock, M.E. Smith, M.R. Baron, P.D. Guidotti, A.M. Wehner, J. A. Shuford, **"Summary of Campaign SGM-8 of the DWPF Scale Glass Melter,"** U.S. DOE Report DPST-87-850, E.I. duPont deNemours & Co. Savannah River Laboratory, Aiken, SC (1987).

36 A.S. Choi, M.E. Smith, K.R. Crow, M.R. Baron, G.F. Rabon, S.L. Goudelock, A.M. Wehner, **"Summary of Campaigns SGM-9 and SGM-10 of the DWPF Scale Glass Melter,"** U.S. DOE Report DPST-88-626, E.I. duPont deNemours & Co. Savannah River Laboratory, Aiken, SC (1988).

37 J.A. Ritter, N.D. Hutson, M.E. Smith, M.K. Andrews, D.H. Miller, and J.R. Zamecnik, **"Integrated DWPF Melter System Campaign Report Coupled Feed Operation,"** U.S. DOE Report WSRC-TR-90-131, Westinghouse Savannah River Company, Aiken, SC (1990)

38 N.D. Hutson, J.R. Zamecnik, M.E. Smith, D.H. Miller, J.A. Ritter, **"Integrated DWPF Melter System (IDMS) Campaign Report: Mercury Operation,"** U.S. DOE Report WSRC-TR-91-363, Westinghouse Savannah River Company, Aiken, SC (May 22, 1991).

39 N.D. Hutson, J.R. Zamecnik, M.E. Smith, D.H. Miller, J.A. Ritter, **"Integrated DWPF Melter System (IDMS) Campaign Report: The First Two Noble Metals Operations,"** U.S. DOE Report WSRC-TR-91-400, Westinghouse Savannah River Company, Aiken, SC (June, 1991).

40 J.R. Zamecnik, N.D. Hutson, M.E. Smith, D.H. Miller, J.A. Ritter, **"Integrated DWPF Melter System (IDMS) Campaign Report - DWPF Cold Run Demonstrations,"** U.S. DOE Report WSRC-RP-93-593,. Rev. 0, Westinghouse Savannah River Company, Aiken, SC (April 21, 1993).

41 M.E. Smith, production records.

42 N.D. Hutson, **"Integrated DWPF Melter System (IDMS) Campaign Report: Hanford Waste Vitrification Plan (HWVP) Process Demonstration,"** U.S. DOE Report, WSRC-TR-92-403, Rev. 1, Westinghouse Savnnah River Company, Aiken, SC (June 11, 1993).

43 N.D. Hutson and J.R. Zamecnik, **"Integrated DWPF Melter System (IDMS) Campaign Report: IDMS Purex-6 (PX6) Operation,"** U.S. DOE Report WSRC-TR-94-0556, Rev. 0, Westinghouse Savannah River Company, Aiken, SC (November, 1994).

44 C.M. Jantzen, **"Relationship of Glass Composition to Glass Viscosity, Resistivity, Liquidus Temperature, and Durability: First Principles Process-Product Models for Vitrification of Nuclear Waste,"** Proceedings of the 5th International Symposium on Ceramics in Nuclear Waste Management, G.G. Wicks, D.F. Bickford, and R. Bunnell (Eds.), American Ceramic Society, Westerville, OH, 37-51 (1991).

45 K.G. Brown, **"Estimating Waste Loading from DWPF SME Analytical Results for Sludge-Only Operation,"** SRTC-GPD-2002-00004 (January 9, 2002).

46 P.G. Walker, **"Melter Performance During the Second SCM-2 Precipitate Hydrolysis Test,"** U.S. DOE Report DPST-85-574, E.I. duPont deNemours & Co., Savannah River Laboratory, Aiken, SC 29808 (August 30, 1985).

47 G.L. Smith, **"Characterization of Analytical Reference Glass-1 (ARG-1),"** U.S. DOE Report PNL-8992, Pacific Northwest Laboratory, Richland, WA (December, 1993).

48 Rept SME-1 #245, LIMS ID 88920, DWPF 221-S Laboratory run with PCCS SME Acceptability Spreadsheet

49 Rept. MFT- #245, LIMS ID 89098, DWPF 221-S Laboratory run with PCCS SME Acceptability Spreadsheet

50 A.D. Cozzi, N.E. Bibler, T.L. Fellinger, J.M. Pareizs, and K.G. Brown, **"Vitrification of the DWPF SRAT Cycle of the Sludge-Only Flowsheet with Tank 40 Radioactive Sludge Using Frit 320 in the Shielded Cells Facility,"** U.S. DOE Report WSRC-RP-2002-00022, Rev. A, Westinghouse Savannah River Co., Aiken, SC (January 31, 2002).

51 T.L. Fellinger, **"Summary of the Shielded Cells Phase I Sludge Batch 2 Rheology Work,"** U.S. DOE Report WSRC-TR-2003-00253, Rev. 0, Westinghouse Savannah River Co., Aiken, SC (July 9, 2003).

52 C.M. Jantzen, N.E. Bibler, D.C. Beam, C.L. Crawford, and M.A. Pickett, **"Characterization of the Defense Waste Processing Facility (DWPF) Environmental Assessment (EA) Glass Standard Reference Material"**, WSRC-TR-92-346, Rev. 1, Westinghouse Savannah River Co., Aiken, SC (June 1994).

53 L28 1.8 **"Determining $Fe^{2+}/Fe^{3+}$ and $Fe^{2+}$/Fe(total) Using the HP8452A Diode Array Spectrometer."**

54 A.D. Cozzi and N.E. Bibler, **"Characterization of DWPF Macro batch (MB3) Glass Samples Received 08/13/2002,"** SRT-GPD-2002-00147, Rev. 0 (November 27, 2002).

55 K.G. Brown, C.M. Jantzen, and J.B. Pickett, **"The Effects of Formate and Nitrate on Reduction/Oxidation (Redox) Process Control for the Defense Waste Processing Facility (DWPF),"** WSRC-RP-97-34, Westinghouse Savannah River Co., Aiken, SC (February 1997).

56 C.M. Jantzen, J.R. Zamecnik, D.C. Koopman, C.C. Herman, and J.B. Pickett, **"Electron Equivalents Model for Controlling REDuction/OXidation (REDOX) Equilibrium During High Level Waste (HLW) Vitrification,"** U.S. DOE Report WSRC-TR-2003-00126, Rev.0, Westinghouse Savannah River Co., Aiken, SC (May 9, 2003).

57 H.D. Schreiber and A.L. Hockman, **"REDOX Chemistry in Candidate Glasses for Nuclear Waste Immobilization,"** J. Am. Ceram. Soc., 70[8], 591-594 (1987).

58 D.K. Peeler, D.R. Best, T.B. Edwards, D.M. Missimer, A.R. Jurgensen**, "Crystallization Potential and Viscosity Assessments for Frit 320/Sludge Batch 2 Glasses,"** GRT-GPD-2003-00124 (September 30, 2003).

59 A. Paul, **Chemistry of Glasses**, Chapman & Hall, London, 293pp. (1982).

60 M.J. Plodinec, **"Long-Term Waste Management Progress Report Small–Scale Electric Melter: II. Slag Formation,"** U.S. DOE Report DPST-78-453, E.I. duPont deNemours & Co., Savannah River Laboratory, Aiken, SC (August, 1978).

61 I.E. Grey and C. Li, **"New Silica-Containing Ferrite Phases in the System $NaFeO_2$-$SiO_2$,"** J. Solid State Chemistry, 69 [1], 116-125 (1987).

62 J.D. Vienna, personal communication, Pacific Northwest National Laboratory (2002).

63 C.M. Jantzen, K.G. Brown, K.J. Imrich, and J.B. Pickett, **"High $Cr_2O_3$ Refractory Corrosion in Oxidizing Melter Feeds: Relevance to Nuclear and Hazardous Waste Vitrification,"** Environ. Issues and Waste Management Technologies in the Ceramic and Nuclear Industries, Vol. IV Ceramic Transactions, V. 93, J.C. Marra and G.T. Chandler (Eds.), American Ceramic Society, Westerville, OH, 203-212 (1999).

64 A.E. VanArkel, E.J.W. Verwey, and M.G. VanBruggen, **"Ferrites I,"** Rec. Trav. Chim. 55, 331-339 (1936).

65 C.M. Jantzen and K.G. Brown, **"Quasicrystalline Approach to Liquidus Temperature Prediction in Nuclear Waste Glasses,"** in preparation for J. Non-Crystalline Solids (WSRC-TR-99-240, Rev. 0).

66 I.S. Shaplygin, I.I. Prosychev, and V.B. Lazarev, Zh. Neorg. Khim 26 [11] 3081-3083 (1981).

67 H. Baker (Ed.), et. al, **"ASM Handbook, V. 3 Alloy Phase Diagrams,"** ASM International, (1992).

68 R.S. Roth, T.Negas, L.P. Cook, **"Phase Diagrams for Ceramists, Vol. IV,"** American Ceramic Society, Westerville, OH, Figures 5014 and 5015 (1981).

69 H.D. Schreiber, F.A. Settle, P.L. Jamison, J.P. Eckenrode, and G.W. Headley, **"Ruthenium in Glass-Forming Borosilicate Melts**," J. of the Less Common Metals, v. 115, 145-154 (1986).

70 P.T. Sarjeant and R. Roy, **"A New Approach to the Prediction of Glass Formation,"** Mat. Res. Bull., 3, 265-280 (1968).

71 Technical Data Summary for the Defense Waste Processing Facility Sludge Plant, U.S. DOE Report DPSTD 80-38-2, E.I. duPont deNemours &Co., Aiken, SC (September, 1982).

72 J.P. Mosley, **"Calculated Physical Properties of SRP Waste Glasses Using Frit 131,"** U.S. DOE Report DPST-80-724, E.I. duPont deNemours &Co., Aiken, SC (December 18, 1980).

73 P.D. Soper and D.F. Bickford, **"Physical Properties of Frit 165/Waste Glasses,"** U.S. DOE Report DPST-82-899, E.I. duPont deNemours &Co., Aiken, SC (October 5, 1982).

74 K.R. Routt, personal communication to C.M. Jantzen, June 14, 1982.

75 D.R. Uhlmann and H. Yinnon, **"The Formation of Glasses**" in Glass Science and Technology, V.1, 1-47 (1983).

76 K.L. Luthra, "**A Comparison of the Mechanism of Oxidation of Ti- and Ni-base Alloys**," Environ. Eff. Adv. Mater., (R.H. Jones and R.E. Ricker, Minerals, Metals and Materials Society, Warrendale, PA, 123-131 (1991).

77 A.D. Pelton, H. Schmalzried, and J. Sticher, J. Phys. Chem. Solids, 40 [12], 1103-1122 (1979) see also Phase Diagrams for Ceramists Figure 6270, Vol VI, American Ceramic Society, Westerville, OH (1987)

78 A. Muan and E.F. Osborn, **"Phase Equilibria Among Oxides in Steelmaking,"** Addison-Wesley Publ. Co., Reading MA (1965).

79 C.M. Jantzen and J.B. Pickett, **"Vitrification of M-Area Mixed (Hazardous and Radioactive F006 Wastes: I. Sludge and Supernate Characterization,"** U.S. DOE Report WSRC-TR-94-0234, Westinghouse Savannah River Co., Aiken, SC (August, 2001).